PERGAMON

Materials Science in Semiconductor Processing 2 (1999) 103–147

MATERIALS SCIENCE IN SEMICONDUCTOR PROCESSING

Review

Characterization and production metrology of thin transistor gate oxide films

Alain C. Diebold[a,*], David Venables[b], Yves Chabal[c], David Muller[c], Marcus Weldon[c], Eric Garfunkel[d]

[a]*SEMATECH, Inc., Austin, TX 78741, USA*
[b]*North Carolina State University, Raleigh, NC 27695, USA*
[c]*Bell Laboratories, Lucent Technologies, Murray Hill, NJ 07974, USA*
[d]*Department of Chemistry, Rutgers University, Piscataway, NJ 08854, USA*

Abstract

The thickness of silicon dioxide that is used as the transistor gate dielectric in most advanced memory and logic applications has decreased below 7 nm. Unfortunately, the accuracy and reproducibility of metrology used to measure gate dielectric thickness during manufacture of integrated circuits remains in some dispute. In addition, detailed materials characterization studies have resulted in a variety of descriptions for the oxide-interface–substrate system. Part of the problem is that each method measures a different quantity. Another related issue concerns how one should define and model the critical dielectric/substrate interface. As scaling continues, the interface between silicon dioxide and silicon becomes a larger part of the total thickness of the oxide film. Although materials characterization studies have focused on this interface, there have been few attempts to compare the results of these methods based on an understanding of the models used to interpret the data. In this review, we describe the physical and electrical characterization of the interfacial layer. Infrared absorption data are reviewed and previous interpretations of the LO/TO phonon shifts as a function of oxide thickness are refined. We correlate the available results between physical methods and between physical and electrical methods. This information is essential to inclusion of an interfacial layer in optical models used to measure silicon dioxide inside the clean room. We also describe some characterization issues for nitrided oxides. © 1999 Elsevier Science Ltd. All rights reserved.

Contents

* Corresponding author. Tel.: +1-512-356-3146; fax: +1-512-356-7640.
E-mail address: alain_diebold@sematech.org (A.C. Diebold)

1369-8001/99/$ - see front matter © 1999 Elsevier Science Ltd. All rights reserved.
PII: S1369-8001(99)00009-8

1. Introduction

The 1997 National Technology Roadmap for Semiconductors indicates that the first shipments of integrated circuits at the 150 nm technology generation will occur in 2001. The transistors are expected to use a gate dielectric with capacitance equivalent to 2–3 nm of silicon dioxide. This trend requires in-line thickness measurement techniques to be capable of monitoring the manufacturing process for 2 nm silicon dioxide, oxynitride or stacked oxide/nitride dielectrics. The total number of atomic layers of a 2 nm silicon dioxide film is so small that an interfacial layer will be a significant part of the total oxide thickness. Considering the importance of thin gate dielectric films, it is surprising that the film–substrate interface is rather poorly understood. In this paper, we review local (atomic level) characterization methods and data for the film and interface region. We then relate this developing understanding to models used to describe currently accepted in-line metrology such as ellipsometry and capacitance–voltage measurements.

It is difficult to fundamentally characterize interfaces using ellipsometry in the visible wavelength range due to the long wavelengths (between ~400–800 nm) and the small optical path length differences that very thin films such as interfaces or nitrided layers (<2 nm) impart. Therefore, we take the approach that materials characterization studies provide atomic/localized information that allows us to determine physically realistic models that can be used by ellipsometry and capacitance–voltage methods. These methods are used for routine, clean room based metrology during integrated circuit manufacturing. This 'in-line' metrology must be capable of measuring many wafers per hour while maintaining the precision required for statistical process control. Another consideration for in-line metrology is that ellipsometry can monitor gate dielectric uniformity and thickness before complete fabrication of the transistor that is required for electrical measurements. One of the advantages of using ellipsometry and capacitance–voltage for in-line measurements is that they average over large areas (relative to atomic dimensions) and can simply be interpreted in terms of slab layers, characterized by dielectric constants $\varepsilon_{\text{layer}}$. These models are used to interpret the results of several techniques that, while all sensitive to ε, probe the dependence of ε in different frequency regions (optical for ellipsometry and dc for capacitance measurements). To adequately monitor process variation in a production environment, the precision (6σ) of the measurements must be about 10 times the tolerance required for the process. The tolerance for gate dielectric thickness is about 8% of the film thickness [Ref. SIA roadmap] expressed as six times the standard deviation, i.e. 6σ. To obtain a precision to tolerance ratio of 0.1 for 2–3-nm-thick films thus requires a measurement precision of ~0.02 nm, 6σ. The precision definition used here contains both short- and long-term measurement variation. Precision numbers of <0.02 nm (6σ) are only achievable by averaging over large areas. It is important to remember that ultimately

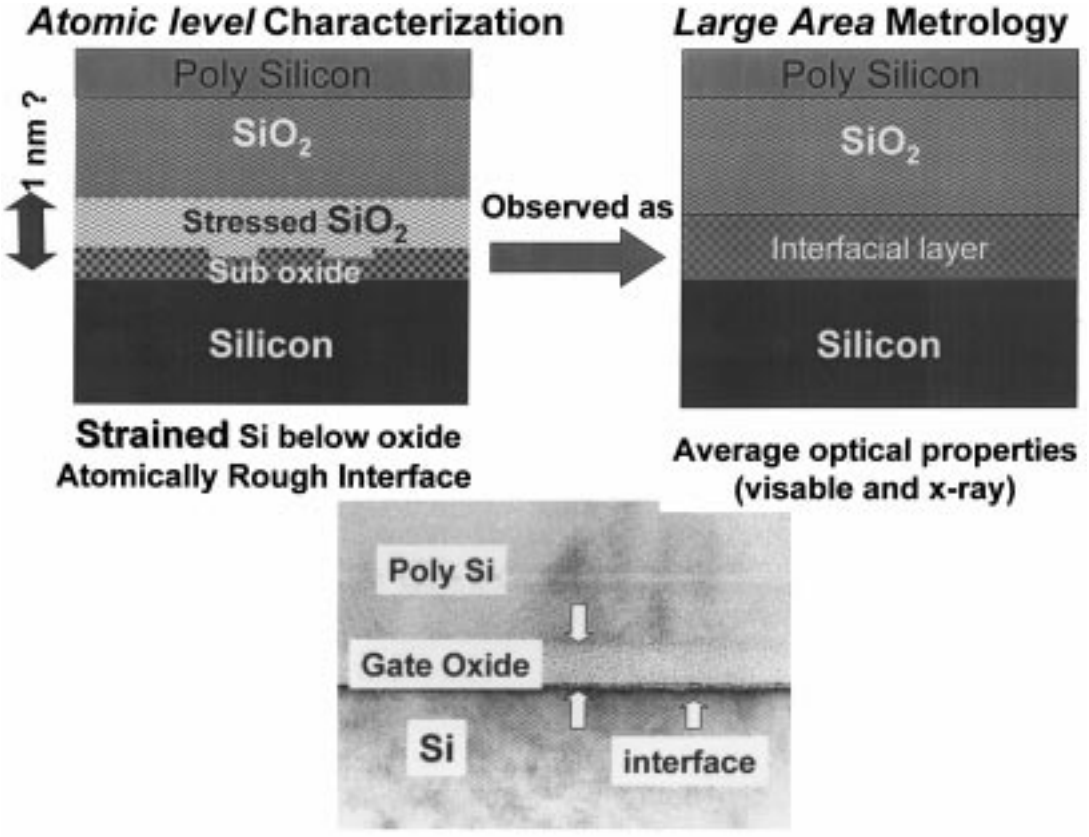

Fig. 1. Model of interface between Si and SiO_2 and TEM Micrograph of a ~3 nm thermal oxide on Si(001).

metrology is intended to insure that the gate dielectric has a constant capacitance to minimize the spread in threshold voltage across a chip, across the wafer and from wafer to wafer. This is the motivation for also examining the connection between the optically measured film thickness and the capacitance measured by C–V. Other metrology issues are out of the scope of this review. This includes 'pinholes' or the nonstatistical very low probability Si intrusions into the gate that may dominate tunneling.

Before presenting a detailed review, it is useful to describe some of the models and problematic issues concerning the interfacial region. The interface can loosely be defined as the transition region between the bulk crystalline silicon and the bulk silicon dioxide film. The interface can contain silicon and oxide components. Some of the important issues that have been discussed for many years include (i) the existence and magnitude of strain in the Si and SiO_2 near-interfacial layers, (ii) the existence and amount of sub-oxides in the SiO_2 near interface and (iii) the extent of roughness (usually defined by roughness in the final plane of ordered substrate Si). The existence of one or more ordered layers of SiO_2, has never been confirmed and will not be discussed in this paper. These models are used to interpret the results of several techniques that, while all sensitive to ε, probe the dependence of ε in different frequency regions (optical and dc for ellipsometry and capacitance measurements). When comparing various techniques, several factors must be kept in mind: sensitivity to different spatial wavelengths of surface roughness and sample preparation conditions and crystal orientation. With these factors in mind, comparison is possible. High spatial resolution probes have provided a picture of the atomic order at the interface, although sometimes with conflicting interpretations. Some recent scanning transmission electron microscopy (STEM) [1] and medium energy ion scattering (MEIS) [2–3] results indicate that there is a small increase in spacing of the (100) lattice planes close to the interface. TEM micrographs of thin oxide films often show a slight roughness at the interface as shown in Fig. 1 [4]. The chemical bonding at the interface has also been studied. A substoichiometric oxide has frequently been reported in X-ray photoelectron spectroscopy (XPS) studies of thin oxide layers [5]. In addition, a recent XPS study has reported that the oxide interface region consists of 0.3 nm of sub-oxide on the silicon and 0.7

nm of slightly denser silicon dioxide above the suboxide layer [6]. Previous infrared spectroscopy measurements have shown a shift in the frequency of the optical phonon like transitions that has been interpreted in terms of a stressed oxide layer at the interface [7–10]. In this paper, we present previously unpublished infrared measurements of the phonon shift and reevaluate the contribution of stress to the observed phonon shift. We conclude that only a small part of the shift can be attributed to a stressed oxide. The data is consistent with the presence of substoichiometric oxides at the interface and some stress. Furthermore, there is chemical inhomogeniety that extends several angstroms above the substrate. Large area measurements provide a layer like (slab) picture of the interface. Atomic scale roughness would be very difficult to avoid over the many microns squared area measured by ellipsometry or X-ray reflectivity (XRR). In a simplified slab model, the interfacial roughness can be considered a thin slab layer with a mix of substrate and film optical properties. The mix of properties may be different for ellipsometry and XRR due to different spatial wavelength sensitivities. XRR measurements have been interpreted as showing a interfacial region of about 1 nm when the data is modeled using a thin layer having an increased density over that of the bulk oxide or silicon substrate [11,12]. The XRR measurements are strong evidence for a stressed oxide. Spectroscopic ellipsometry data for thin oxide films can be interpreted in terms of an optical model that has a thin interfacial layer (slab) with effective dielectric properties that are obtained by averaging silicon and oxide refractive indices [13–16]. This interfacial layer can account for both microroughness and strain. To date, no one has pursued an optical model that accounts for interfacial microroughness, the suboxide above the silicon and the denser oxide layer. Optical absorption in the vacuum ultraviolet has also been used to characterize the Si/SiO_2 interface [17]. This data has been interpreted as evidence of a high number of Si–Si bonds ($\sim 8 \times 10^{14}/cm^2$) in the oxide that exists in the 1.4 nm above the substrate silicon [17]. A model-based summary of the above discussion is shown in Fig. 1. Some aspects of this model such as the evidence for the stress oxide layer will be questioned in this review.

Comparison of electrical and optical metrology methods requires use of models and dielectric constants. As discussed in the last section, electrical methods consider the dielectric layer to be a slab with the frequency-dependent dielectric constant to have the same value as the static dielectric constant of bulk silicon dioxide. In-line ellipsometric measurements can incorporate optical models that include an interface layer. Measurements of the dielectric constant of thin oxides have concluded that the band gap of thermally grown oxides thicker than 2.3 nm is 8.95 eV, regardless of the thickness [18]. Furthermore, some researchers have concluded that the stress in the oxide next to the interface is relieved after further heat intensive processing including the deposition of polysilicon for the gate electrode. Clearly, the dielectric properties (for frequencies associated with optical measurements) of the interface layer are different than the bulk oxide. In order to correlate optical and electrical measurements, we must determine the high frequency properties of thermally grown oxide film including the interface and relate them to the low frequency dielectric properties of the interface after deposition of the poly-silicon gate electrode. These same issues extend to nitrided oxides and other alternate gate dielectric materials.

In this paper, we critically review some of the experimental data that has been used to characterize the presence of the interfacial layer. We present a convenient optical model for the interfacial region and make the connection between models for interpreting optical measurements and capacitance–voltage measurements [19], while stressing that a consensus model for the interface is not yet available. In Section 2, we discuss characterization at atomic dimensions by STEM and MEIS. In Section 3, we discuss XPS, optical second harmonic and infrared spectroscopy analysis of the atomic bonding of interfacial oxygen. Previously unpublished infrared measurements and a thorough discussion of the cause of shifts in the observed phonon frequencies is presented. X-ray and neutron reflectivity characterization of thin oxide samples is described in Section 4. In Section 5, we describe the optical models that result from this data and ellipsometry of thin oxides. In Section 6, we attempt to correlate optical and electrical measurements of oxide thickness.

2. STEM and MEIS characterization of oxide film structure at atomic dimensions

In this section, we describe STEM and MEIS characterization of the silicon lattice that lies next to the oxide layer.

2.1. Scanning transmission electron microscopy (STEM)

STEM imaging is different from conventional high resolution TEM imaging. In conventional high resolution TEM (HRTEM) imaging, a nearly parallel electron beam travels through the sample and the direct (transmitted) beam and the diffracted beams are allowed to interfere with one another to form a 'lattice' image. The resulting image reflects the periodicity of the crystal lattice since the lattice acts essentially as a

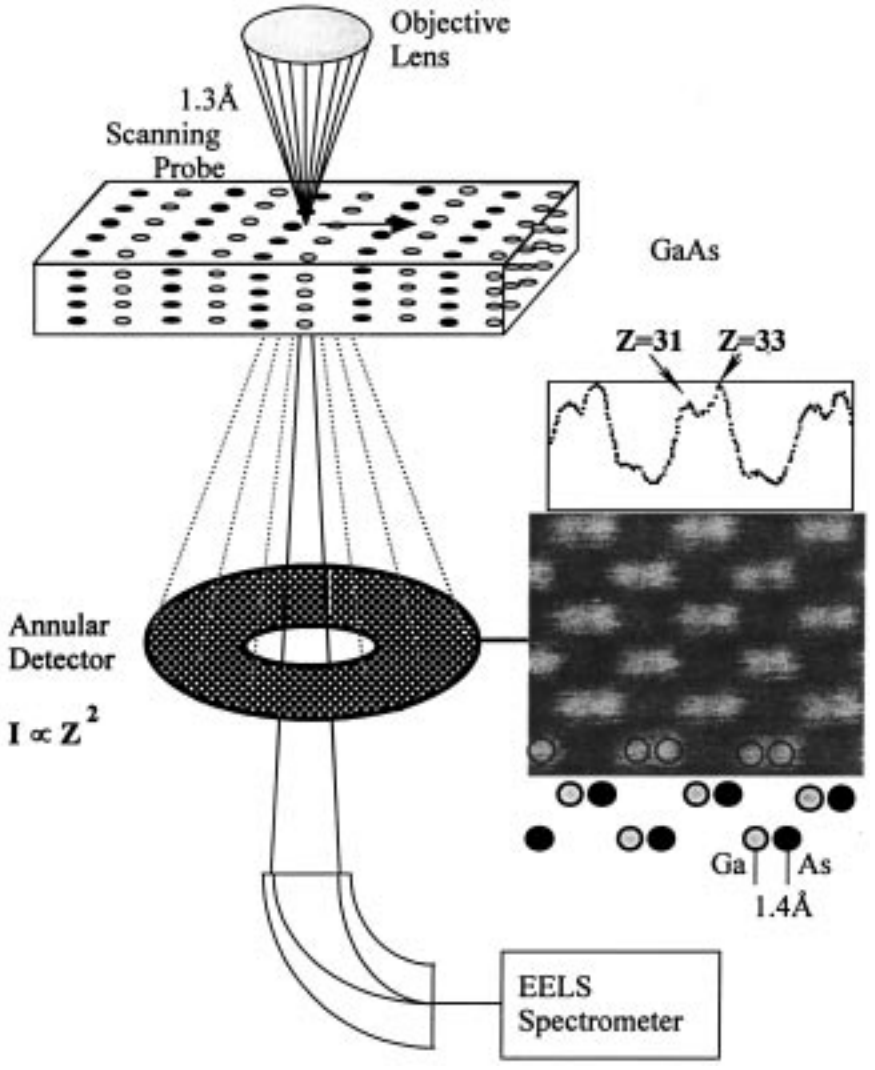

Fig. 2. Block diagram of an annular dark field-scanning transmission electron microscope (ADF–STEM). Figure first published in Ref. [1]. Reproduced with permission.

phase grating. However, image interpretation can be complicated by inversions of contrast, which depend on the specimen thickness and the objective lens defocus and additional interference effects (Fresnel fringes) at the interface between the crystalline substrate and the amorphous dielectric. In contrast, high resolution images obtained in a scanning transmission electron microscope equipped with an annular detector can be much simpler to interpret. This simplicity is a direct result of the fact that only electrons scattered through 'large' angles are used to form the image, so that interference effects contribute less to the image. The STEM image is consequently far less sensitive (although not immune) to specimen thickness variations, tilt and defocus. A block diagram of a STEM is shown in Fig. 2. In this mode of operation the electron beam is focussed to a very fine spot (<2 Å is feasible). This fine probe is scanned over the specimen and transmitted electrons scattered through large angles strike the annular detector. Since the maximum scattering occurs when the electron probe is centered over a column of atoms, the columns appear bright in the image. Little scattering occurs when the probe is centered over a channel between atomic columns, so that these areas appear dark. In a perfect crystal, atoms with higher atomic number, Z, produce more scattering, so that the intensity of the bright spots in the image can be related to the atomic composition of the corresponding column of atoms in the sample. Annular dark field (ADF) STEM is sometimes known

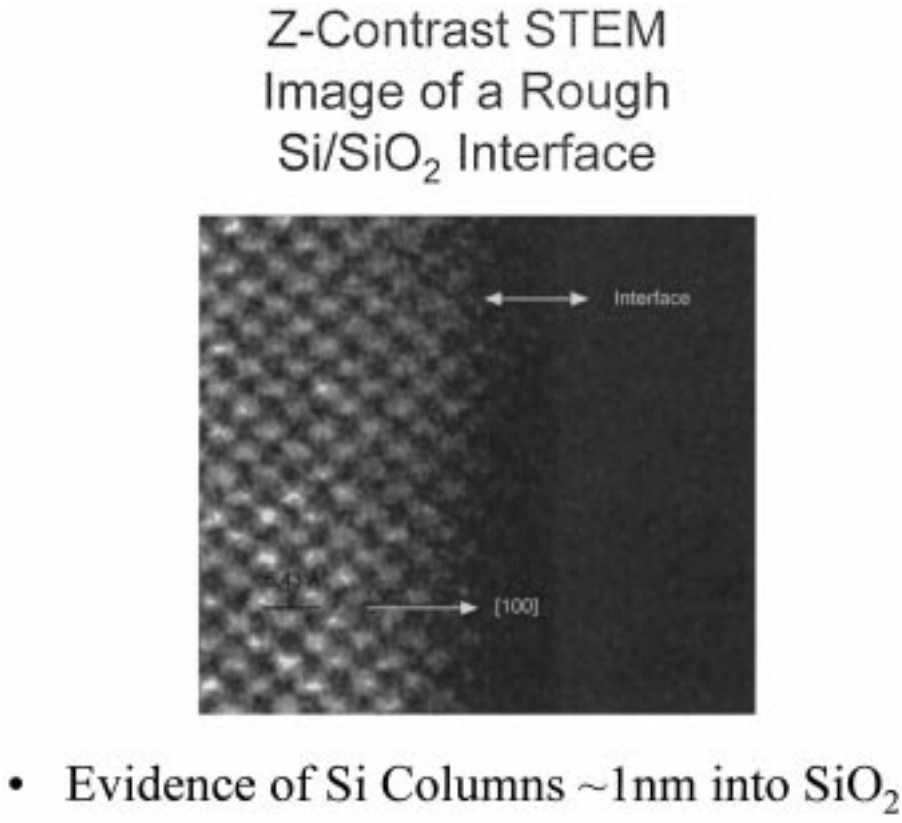

Fig. 3. Z contrast image produced by ADF–STEM. Figure first published in Ref. [1]. Reproduced with permission.

as '*Z*-contrast' imaging because of this atomic-number sensitivity. However, the image intensity is also affected by strain contrast and the channeling of the probe which is useful for detecting light dopant atoms. Amorphous materials (such as the gate dielectric) do not have periodically arranged atomic columns or channels so they appear as regions of uniform intensity. An ADF–STEM image of si/siO_2 interface is shown in Fig. 3. Line profiles through STEM images of thin specimens provide both the gate oxide thickness and the interface roughness (averaged along a column of atoms parallel to the electron beam). The bulk silicon lattice provides a precise, absolute calibration for the gate thickness.

Apart from the manner in which the image is formed (scanning versus parallel illumination), the main difference between STEM and HRTEM imaging is the contrast mechanism. For very thin specimens, HRTEM imaging is primarily a coherent, phase-contrast imaging technique while STEM imaging is an incoherent, amplitude-contrast technique. The incoherent nature of the ADF image (which measures the square of the electron wave function) largely removes the contrast reversals present in phasecontrast HRTEM. ADF imaging also trades off higher resolution for reduced contrast. Consequently, unprocessed ADF images always look more 'blurry' than HRTEM images, which in turn are artificially sharpened by the microscope. (The HTREM suppresses the lower frequencies in the image, while ADF enhances them). Although the ADF image does not look as sharp, the point-to-point resolution is roughly 50% better than CTEM for the same beam voltage and instrumental abberations. A commercial, 200 kV field-emission-analytical-microscope has a HRTEM point-to-point resolution of 2.3 Å. The same instrument when operated as a STEM has a point-to-point resolution of 1.8 Å or better (the limit being source brightness).

The STEM mode is also useful for imaging very thick specimens (1–5 μm thick). One of the major weaknesses of electron microscopy is that it can often take 4 or more h to prepare a specimen thinner than 1 μm. Ideally, the specimen thickness for conventional TEM should be 300 nm or less (and less than 50 nm for atomic resolution TEM). Interpretable, atomic resolution STEM images can still be obtained in 100–200 nm thick specimens. In specimens thicker than 1 μm (which can be prepared in less than 1 h), the STEM resolution is degraded to about 1 nm. Since most of the scattered electrons are collected by the annular

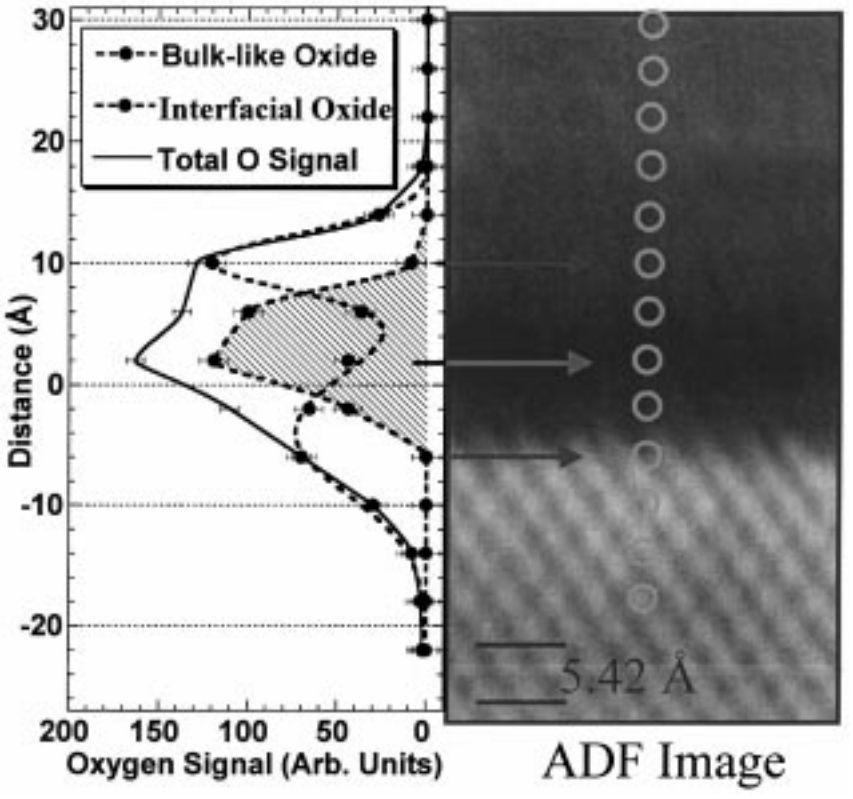

Fig. 4. Electron energy loss spectrum from STEM analysis of O in ultrathin SiO_2. (a) The oxygen profile measured by EELS in a STEM from an ultrathin gate oxide. The presence of interfacial states changes the shape of the O–K edge, which is used to map bonding changes across the oxide. (b) The corresponding ADF–STEM image, where the circles indicate the positions at which the O–K edge EELS spectra were recorded. Figure courtesy of D.A. Muller, from Ref. [21].

detector, a strong signal is still obtained. This is in contrast to a conventional TEM, which relies on collecting the electrons in the unscattered beam, which is depleted at these thicknesses.

One attraction of ADF–STEM imaging over HRTEM is in obtaining quick, readily interpretable (if only qualitatively) images by relying on the enhanced chemical sensitivity ($Z^{1.7}$ for ADF versus $Z^{0.66}$ for HRTEM) and reduced sensitivity to instrumental and scattering artifacts. A second and very important role for annular-dark-field imaging is in positioning the electron probe for spectroscopic techniques such as electron energy-loss spectroscopy (EELS) or X-ray analysis, which can be performed simultaneously with ADF measurements. This has made it possible to perform atomicscale energy-loss spectroscopy at silicon/silicon dioxides interfaces [20]. Batson has identified Si^{2+} defects at a the interface between steamgrown silicon dioxide and an [001] Silicon substrate. Timp and coworkers have mapped the oxygen distribution across 1–2 nm thick gate oxides in MOSFETS, including the width of the interface as shown in Fig. 4. EELS can also be used to profile oxynitride thin films, measuring not only the N/O ratio, but also the local bonding and electronic structure. At atomically abrupt interfaces, the spatial resolution of EELS is about 0.2 nm. However, as the interface is viewed in projection, interface roughness greater than 0.2 nm will degrade the spatial resolution (Fig. 5)

Duscher et al. [1] have applied STEM techniques to the analysis of the interfacial region between silicon and silicon dioxide. On the basis of Z-contrast images of the cross section of a thermal oxide, they conclude that there is no evidence for a crystalline oxide phase at the interface as has been reported by others. In addition, they show that information about the strain due to the presence of an oxide layer can be determined from Z-contrast images, as shown in Fig. 6. The electrons are scattering from atoms that are constantly in motion and both the atomic displacement from bulk positions (strain) and the vibrational amplitude at room temperature contribute to the intensity and location of the bright spots in the image [1]. These and other effects can be distinguished using images obtained from lower angle scattering and greater angular resolution [1]. An exponentially decreasing strain

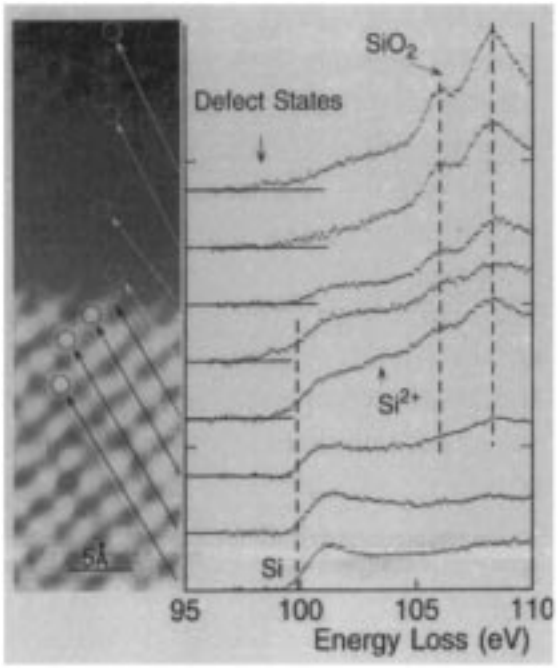

Fig. 5. Electron energy loss spectrum from STEM analysis of Si in ultrathin SiO_2. Electron energy loss-spectroscopy is used to map changes in the Si–L edge across an interface between [001] silicon and a steam grown oxide. The Si^{2+} formal valence state is detected at the interface. The annular dark field image on the left is used to position the electron beam for spectroscopy. (From Ref. [20]. Reproduced with permission.)

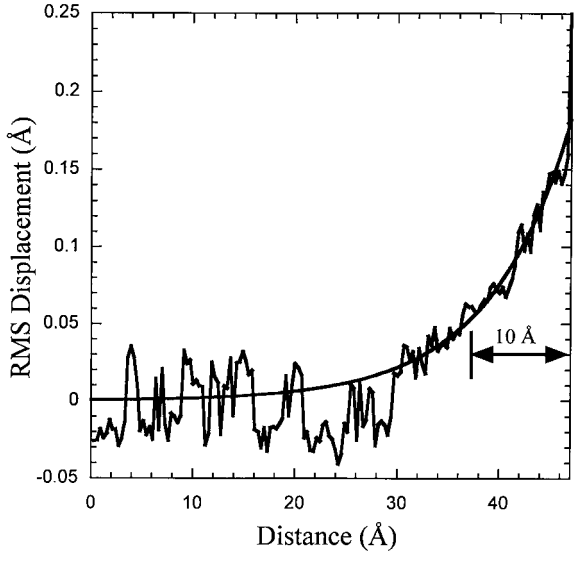

Fig. 6. Strain versus depth below the Si/SiO_2 interface. Figure first published in Ref. [1]. Reproduced with permission.

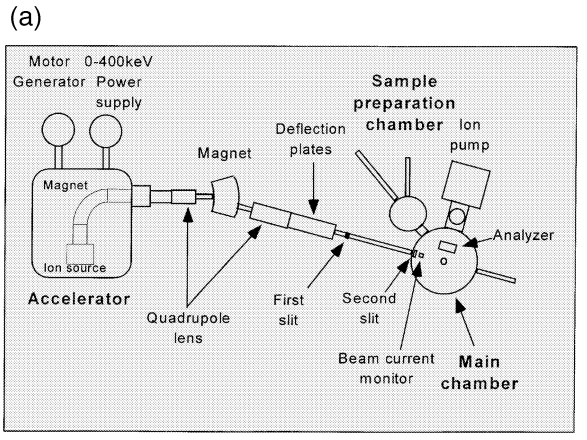

Layout of accelerator, beam line, and chambers

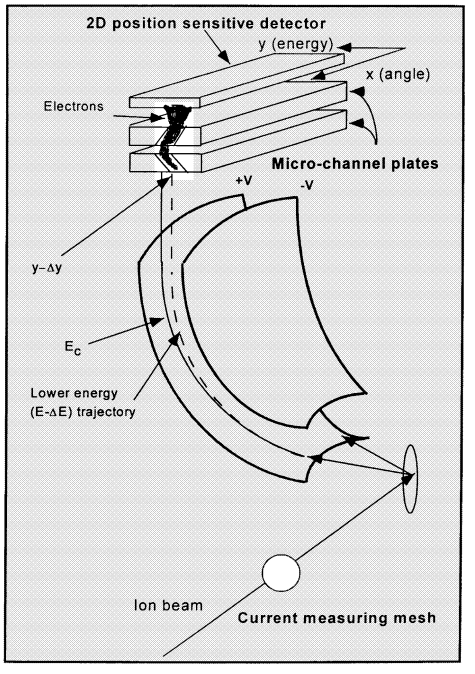

Fig. 7. Block diagram of (a) MEIS system and (b) high resolution detector. Figures first published in Ref. [34] and reproduced with permission.

was observed over about 1 nm for a rather rough, thermally oxidized Si(111) surface.

There is a clear need to apply stain analysis to oxide layers grown on Si(100) using processes representative of CMOS transistor fabrication. However, it is important to note that the relationship between the strain observed in the very thin samples used in STEM or TEM and that observed in wafer samples is not well understood. In addition, strain measurement using

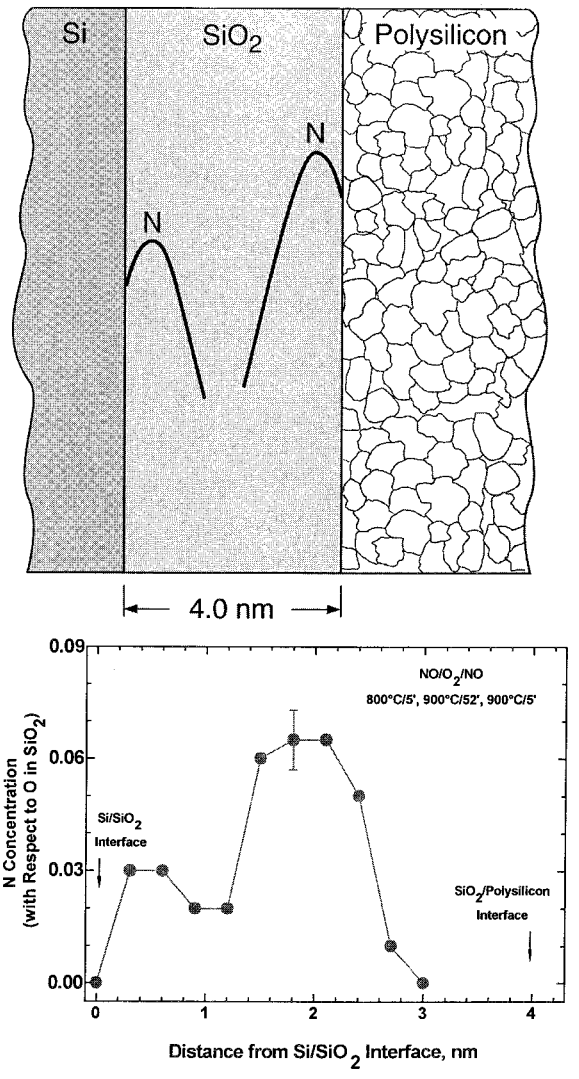

Fig. 8. MEIS depth profile showing nitrogen position and concentration for a nitride/oxide/nitride sample.

ADF–STEM requires further development. The increased intensity at the interface could be either from probe dechanneling at the rough interfaces as the probe enters and leave the oxide *or* from strain in the bulk silicon as Duscher and coworkers suggest. However, these two effects cannot be distinguished or even quantified until further, sufficiently accurate modelling of the beam-specimen interactions have been performed.

If one refers to the TEM electron micrograph in Fig. 1, atomic level microroughness can be observed over the length range of ~100 nm. This results in an uncertainty when a TEM micrograph is used to calibrate optical measurements. One can imagine that there is at least ~0.05 nm uncertainty in how two

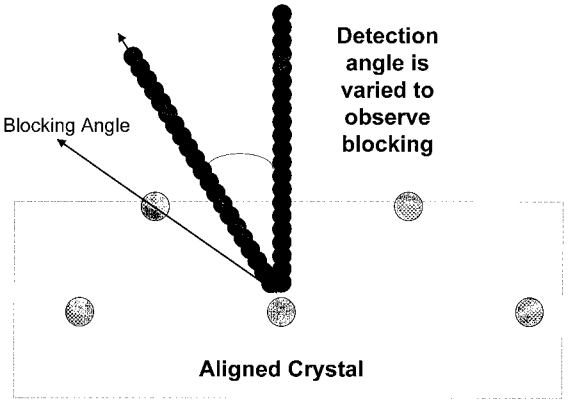

Fig. 9. Origin of blocking dip in MEIS.

people (or multiple measurements on a single micrograph) might draw a line at the interface and then determine oxide thickness. This uncertainty is rather large when compared to that required for calibration of optical measurements.

2.2. Medium energy ion scattering

MEIS has been used to examine the interfacial structure, strain, growth behavior and stoichiometry of thin gate oxide films. MEIS is a lower energy version of Rutherford backscattering in which a high energy and angular resolution detector is used to obtain detailed information about atomic structure and composition in the top 50–200 Å of the sample. Groups at IBM, Rutgers University and the Korea Research Institute for Science and Standards have used MEIS to characterize gate dielectrics [2]. The Rutgers MEIS system is shown in Fig. 7.

In a typical MEIS experiment, ~100 keV protons are used as a probe beam and the protons scattered from an oriented sample are detected with high angular and energy resolution. The use of a high energy resolution detector and 100 keV energies (instead of MeV energies) greatly increases surface sensitivity [22–24,104]. The increase in surface sensitivity is also useful for quantification of trace surface contamination and is the basis of the heavy ion backscattering spectrometer (HIBS) developed by Doyle, Knapp and Banks [23,112]. The time-of-flight ion detector used in HIBS (and medium energy backscattering spectrometry, MEBS) is designed to increase counting rate and does not have the energy or angular resolution of MEIS, while the detector used for MEIS is not suitable for trace contamination analysis. The physics of backscattering is well understood and a depth profile of elemental constituents in the sample can be calculated from MEIS data. Unfortunately, MEIS analysis of a single sample may require ~10 h to get reasonable stat-

istics. Because protons are used as a probe in MEIS, elements heavier than hydrogen can be characterized in the sample [23,104]. Therefore, one can determine the position and concentration of nitrogen in very thin oxide/nitride (or more complex) stacks using MEIS as shown in Fig. 8 [25–27].

Ions can channel between rows of atoms. Ion channeling and blocking methods can be used to study surface or interface structure and the high energy and angular resolution of MEIS make it an excellent tool for such studies. In these studies, the change in backscattered intensity is measured as a function of backscattering angle. At certain angles, surface atoms will block the backscatter of probe beam ions from subsurface atoms [28]. The angle at which the backscattered intensity is a minimum is considered the blocking angle as shown in Fig. 9. Surface structure is determined by the change in blocking angle between a perfect bulk crystal and the reconstructed surface [28]. *Blocking MEIS studies for an amorphous overlayer on a crystalline substrate see all of atoms in the amorphous region and the first few atomic layers of ordered substrate, while the STEM, usually looking in cross section through a 10–30-nm-thick slice, characterizes rows of atoms from the bulk to the ordered layers in the interface*. Si(001) will have a blocking dip in MEIS along the [111] direction when the probe beam is aligned close to an [001] incident direction as shown in Fig. 9. The blocking dip for [001] direction is studied by aligning the probe beam along the [111] direction. The change in angle for the minimum backscattered intensity was studied as a function of probe beam energy for a 5.5 nm thick thermal oxide on Si(001) by Moon et al. [2,3]. Based on their data, the (100) interlayer distance was found to increase by 0.0011 nm which corresponds to a strain of ~1%. There was no shift in the lattice perpendicular to the surface normal since the [001] blocking dip did not shift [2,3].

Thus both Pennycook's STEM and the KRISS MEIS data are interpreted as showing an increase in the spacing between the lattice planes next to the interface with the oxide. The STEM data for thermal oxide on Si(111) indicated a >0.01 nm increase for the lattice plane closest to the interface while the MEIS data showed a ~0.001 nm increase for the Si(100) lattice plane at the interface. A logical next step is to compare STEM and MEIS data taken using pieces of the same wafer having a 2–3 nm thermal oxide grown using a typical transistor gate oxidation process. Comparison of this data may also allow initial correlation of the change in strain when a sample is thinned.

MEIS data have also been interpreted to yield the density of the interfacial layer. MEIS determines the areal density (atoms/cm^2) of silicon and oxygen atoms. The ion stopping power (eV/⊕) can only be known or determined if the bulk density is also known; only then can a film thickness be accurately determined. Moon has indicated that the error in the density of the interface layer is larger (~10%) than the difference in the densities of bulk silicon and silicon dioxide. The thickness of the interlayers in a 5.5 nm (and a 3.0 nm) thick oxide layer was estimated to be 1.3 nm (1.23 nm). These estimations are based on a specific value for the areal density of compressed silicon.

In Fig. 10, data from the Rutgers group are presented showing the Si versus O yield for different thickness films. Although the bulk of the SiO_2 film shows correct stoichiometry, excess Si is present near the interface in the spectra that cannot be accounted for by a perfectly terminated Si substrate abutting a perfectly amorphous SiO_2 film. The Rutgers group feels that the absolute MEIS depth resolution of the spectra for their films is such that the excess Si may either be in the form of strain in the Si substrate, as argued by the Korean group, or as excess Si in the SiO_2 film as sub-oxides, as discussed below.

3. XPS, optical second harmonic and infrared characterization of the atomic bonding of interfacial oxygen

3.1. X-ray photoelectron spectroscopy

XPS is an accurate ultrahigh vacuum characterization method in which photoelectrons are first generated by bombarding a material with X-rays and then energy analyzed to yield information about elemental composition and in some cases local chemical bonding. XPS can be performed on isolated gas phase atoms and molecules, although it is now most commonly used to analyze material surfaces. Because the mean-free-path of low energy electrons (10–1000 eV) is quite short, photoelectrons generated in XPS that arrive at the electron detector are predominantly emitted from atoms residing within the top ~25 Å of a material; thus the surface sensitivity. From the known photon energy and the measured kinetic energy of a photoelectron, one can roughly determine the initial 'binding energy' of the electron. Because all atoms have unique binding energies for their atoms, the electron energy spectrum of a material can be used to quantitatively determine its elemental composition. Furthermore, if the mean-free-path is known for electrons of a certain energy in a given material, the thickness of a layered layered film of know density can be determined. A closer analysis of the peak positions and shapes can be used to determine the oxidation state (chemical environment) of the atom. Angularly resolved photoelectron spectroscopy can be used to determined the valance band electronic structure of some crystalline solid materials and overlayers and can also be used to

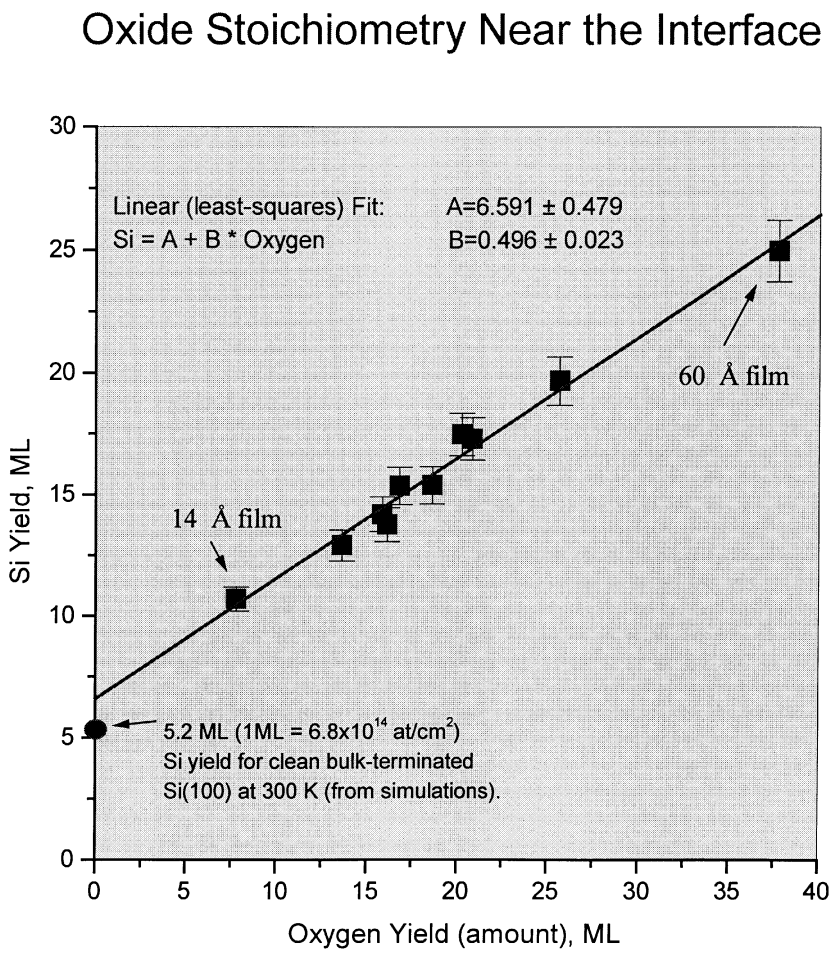

Fig. 10. The silicon MEIS yield plotted against oxygen yield for a series of SiO_2 films grown by rapid thermal oxidation. Approximately 1.4 monolayers (9.5×10^{14} atoms/cm^2) of excess silicon atoms are seen near the interface. Excess silicon may be due to a higher silicon concentration in the near interface silicon oxide and/or silicon substrate distortions Figure first published in Ref. [34] and reproduced with permission.

determine a depth/compositional profile somewhat analogous to what MEIS and SIMS offer. A block diagram of an XPS system is shown if Fig. 11.

The chemical nature of an oxide film and even the interfacial region between a thin oxide layer and its substrate can be characterized by XPS. Although most variants of XPS sample a large area (mm^2–cm^2), it is the local bonding of atoms that determines the spectra. The SiO_2/Si(001) interface has been the topic of numerous studies [5–6,29–40,105]. The consensus interpretation [5–6,29,34,38] of these studies is that in addition to seeing a significant amount of elemental Si and Si^{+4} on the Si substrate and SiO_2 overlayer sides of the interface respectively, some of the Si atoms at the interface are in the Si^{+1}, Si^{+2} and Si^{+3} 'sub-oxide' oxidation states; a thorough analysis of this is given in Himpsel et al. [29] The Si (2p) photoelectron spectra for a thin oxide layer is shown in Fig. 12 along with the standard peak assignment.

At least five issues remain in some dispute resolved concerning the interpretation of photoelectron spectra (background subtraction, peak assignment and uniqueness of fit, mean-free-path and other parameters, the quantity of hydrogen and position of H-shifted peaks and acceptable uses of angularly resolved or integrated methods). One controversy that has existed for over two dozen years, is how to perform a proper background substraction on the spectrum such that the sub-oxide yield can be determined quantitatively. It is precisely the amount of sub-oxide that both the device and the surface science communities need to quantify, if an atomic scale understanding of this critical interface is ever to be known. Some see no crime in using a Shirley background subtraction routine, some use

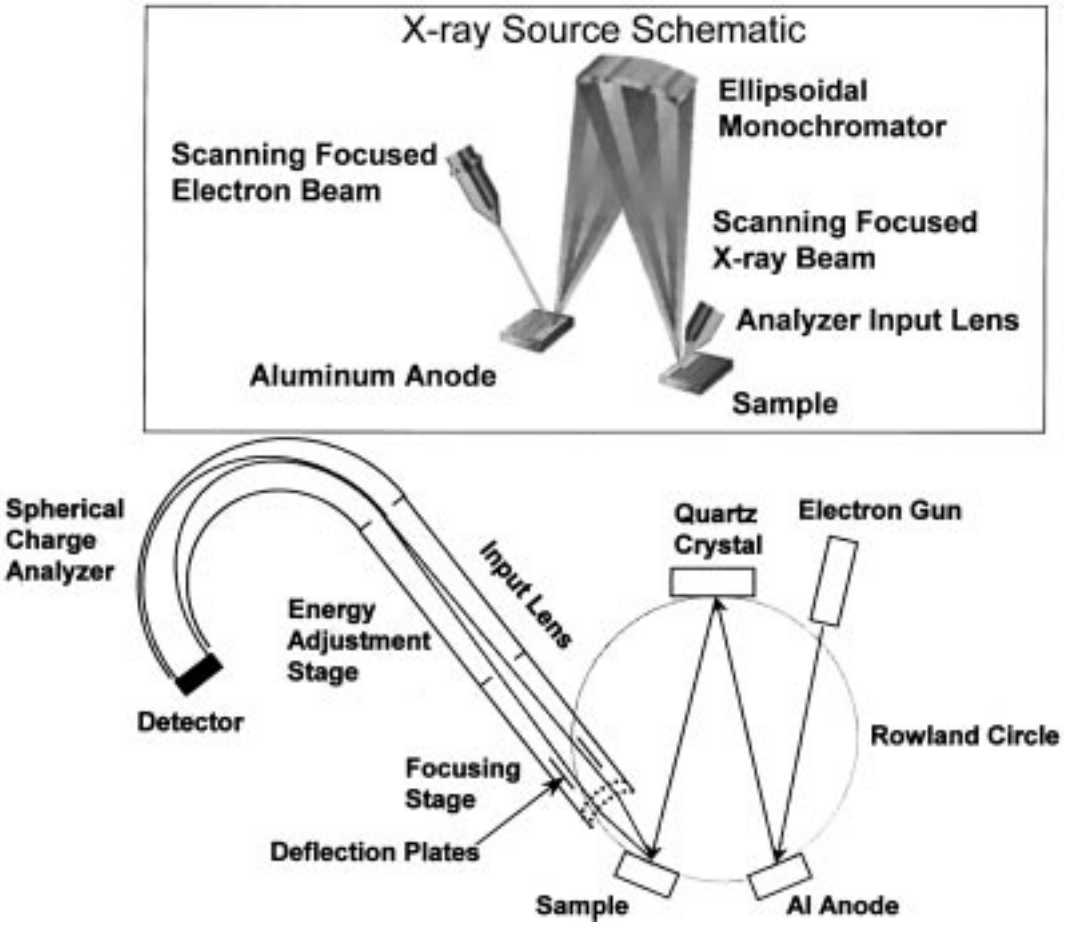

Fig. 11. Diagram of an X-ray photoelectron spectrometer. Figure courtesy of Marlin Braun, Physical Electronics.

more sophisticated methods, while others argue that only synchrotronbased studies can circumvent the intractable background subtraction problems that arise when using Al or Mg Kα X-ray excitation. Signal-to-noise (S/N-problems used to be serious, but with current generation XPS systems (and synchrotron work) this is less problematic. The sub-oxide peak assignments (in terms of both energy position and width) of the photoelectrons emitted between 100.5 and 103 eV binding energy was challenged recently [36,37]. Part of the objection to the traditional sub-oxide interpretation (that the three intermediate oxidation state peaks are linearly spaced in energy between Si and Si^{+4}) is that second-nearest-neighbor electronic effects can be significant in determining the photoemission peak position and are not fully taken into account in the classical model. A new model has been proposed to account for the various peaks in the SiO_2/Si photoemission spectrum and support for the new model from model molecular adsorbates has been demonstrated, however the challenge remains controversial. One ab initio theoretical study has shown that second-nearest-neighbor effects are real but not significant [38]. Another issue is that final state relaxation is a function of distance from the interface and is rarely included in

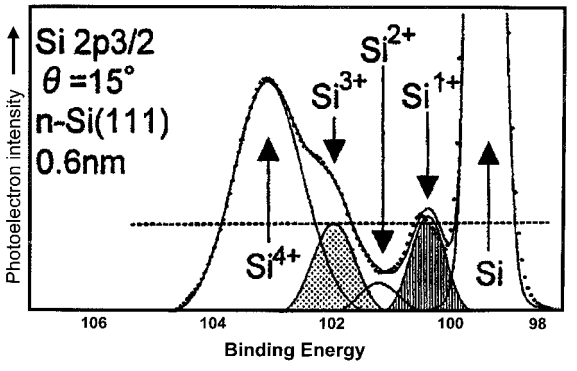

Fig. 12. Oxidation states of Si at the Si/SiO_2 interface. Figure first published in Ref. [5]. Reproduced with permission.

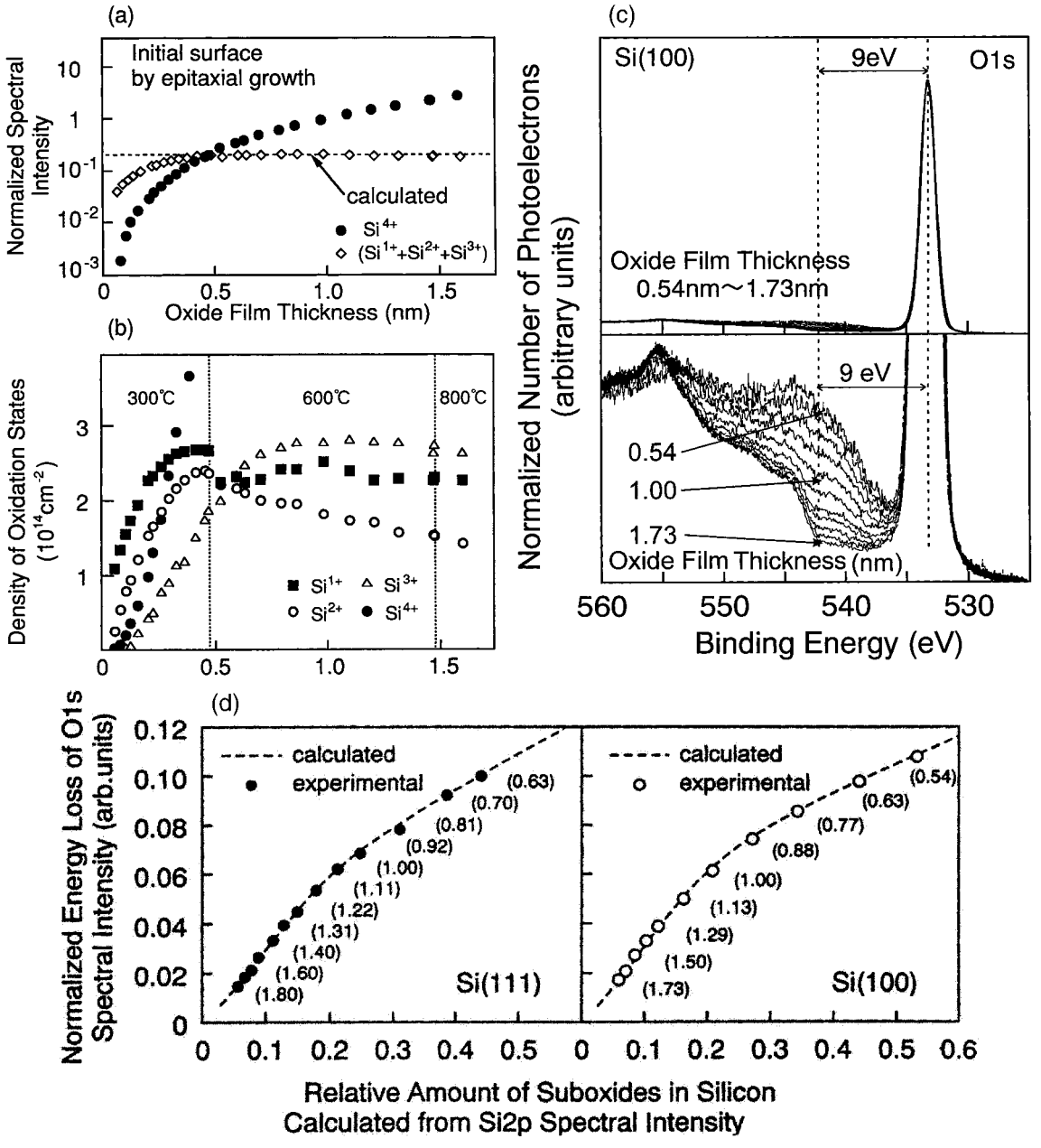

Fig. 13. XPS intensity ratio data showing a transition layer above the sub-stoichiometric oxide. Figure first published in Refs. [6,33,105]. Reproduced with permission. (a) Intensity of Si(+4) and total sub-stoichiometric oxide states versus oxide thickness. (b) Density of oxidation states versus oxide thickness. (c) O (1s) photoelectron intensity for various oxide thicknesses. (d) Plot or the relative amount of O (1s) energy loss versus substoichiometric oxide intensity. Figure first published in Ref. [6] and reproduced with permission.

modeled spectra. *Concerning metrology, both the classical and novel sub-oxide peak interpretations will not significantly change the quantity of sub-oxide that is determined from a given spectrum*; this is more effected by the background subtraction routine. Although the thickness of this sub-oxide at a thermally annealed SiO_2/Si interface has remained controversial, it has narrowed from 10–30 Å claimed by some workers 20 years ago, to somewhere between 1.0 monolayer (which one gets by definition from a perfectly termi-

nated Si/SiO_2 interface) and 2 monolayers [5,33,34,105]. The compositonally-sharp well-phase-segregated interface model with ~1 ML of sub-oxide model has been given strong support in the very accurate work of Hattori et al, while many others are claiming 1.2–2.0 ML of sub-oxide (with the excess stretching 5–10 Å into the SiO_2 film), arguing that the excess is seen by other techniques as well. Unfortunately XPS is probably unique in its ability to quantify sub-oxide concentration; most other methods could easily be seeing strain, roughness, hydrogen or be modeling improperly. The exact amount of this sub-oxide is very important in helping one to better define thickness metrology for ultrathin films. We clearly need to define the interface compositionally as well as structurally, where the latter usually refers to the crystalline to amorphous transition 'plane' as seen for example in TEM. It is quite possible that the compositional and structural interface are not the same. The substoichiometric oxide quantity also needs to be understood by device physicists and engineers who are trying to understand interface electrical defects. Current devices are made with 10^9 defects/cm^2 and this is 3–4 orders of magnitude below the sensitivity of what XPS can observe. Below we describe XPS results from some laboratories that are working on state-of-the-art samples.

Opila et al. have studied the evolution of these sub-oxides with annealing of thin oxide layer formed by RTO [35]. The intensity of the sub-oxide photoelectrons decreased after a 1000°C anneal in Ar. [35]. Electrical characterization of these films showed a 40× decrease in interface state density and a 20× decrease in oxide charge density. Charge to breakdown increased by 2× [35].

Recently, Hattori and coworkers have found that detailed CPS studies of a series of thin oxide layers suggest a 0.7 nm thick densified oxide layer above the 0.3 nm thick sub-oxide layer at the interface with the silicon substrate [6]. The total interfacial layer is found to be about 1 nm which matches the thickness of the interfacial layer observed by XRR [11,12]. Since proof of the existence of a dense oxide layer at the interface is critical to the suggestion of a realistic optical model, we present some of the data interpretation here.

Previous work had shown that the intensity of the Si (2p) photoelectron peaks associated with sub-oxides were sensitive measures of changes in local structure during oxide growth [5,33,105]. In addition, the total intensity of the sum of the sub-oxide peaks increased as oxide thickness went from zero to ~0.5 nm and then the intensity remained constant as film thickness increased from 0.5 to 2 nm. The intensity of the 2p peak associated with silicon dioxide is an indication of oxide thickness when it is normalized to the Si 2p peak from the unoxidized silicon substrate. This is shown in Fig. 13(a). Only the Si (2p) photoelectron spectrum is interpreted in terms of the sub-oxide peaks. The O (1s) spectra intensity at higher binding energies than the main peak is due to energy loss to specific energy states. This is based on electron energy loss spectroscopy based observation of 5.1 and 7.2 eV energy loss peaks that were considered as being characteristic of the interfacial oxide film [30].

It is important to remember that the photoelectrons will be inelastically scattered as the travel from where they originate to the surface. The amount of inelastic scattering will increase as the oxide thickness increases, especially for the photoelectron that come from the interface. For example, a photoelectron originating at the interface of a 5 nm film on silicon is much more likely to be inelastically scattered before it reached the top of the film than is an electron originating at an interface of a 1 nm film on silicon. Presumably, the decrease in the intensity of photoelectrons from O (1s) should change linearly with changes in intensity of the sub-oxide Si (2p) photoelectrons as oxide thickness is increased if the electrons are traveling through a uniform oxide layer [6]. A different functional dependence is observed when a denser oxide layer exists above the sub-oxide layer. The functional form of this curve was theoretically determined for comparison with experiment [6]. Plots were constructed from two ratios by taking data for a series of different oxide thickness'. The ratios were determined as follows [6]. The y-axis is a ratio of intensity of that occurs in the energy region associated with the sub-oxide O (1s) photoelectrons to the intensity of the main O (1s) emission. The O (1s) XPS spectra is shown in Fig. 13(b). Thus, Hattori refers to the photoelectron in the main O (1s) peak as nonscattered and elastically scattered ($I_{el}+I_{nonscatt}$). The intensity that is shifted a few eV from the O (1s) peak are due to inelastically scattered photoelectrons, (I_{inel}) that come from energy losses associated with the sub-oxide layer. The intensity is taken between 3 and 9 eV. This is because the band gap of silicon dioxide films thicker than 2.3 nm has been found to be 8.95 eV independent of thickness [6,18]. Furthermore, XPS studies of the valence band suggest that oxide stress changes the band gap energy [6,18,31,32]. The y-axis is the value of $I_{inel}/(I_{el}+I_{nonscatt})$ for different oxide thickness. The x-axis is the total intensity of the Si (2p) sub-oxide peaks (I_{SiO_x}) divided by the intensity of the Si^{+4} plus I_{SiO_x}, ($I_{SiO_2}+I_{SiO_x}$) [6,33,105]. Thus, the sub-oxide intensity is normalized by all the Si (2p) intensity that does not come from the silicon substrate. As shown in Fig. 13c, the experimental data follows the theoretical curve predicted for an oxide film having a dense (structural transition) layer above the sub-oxide [6]. The curve shows two linear dependencies with the break at 1 nm. When combined with the information shown in Fig. 13(a), infrared and X-ray reflectivity stu-

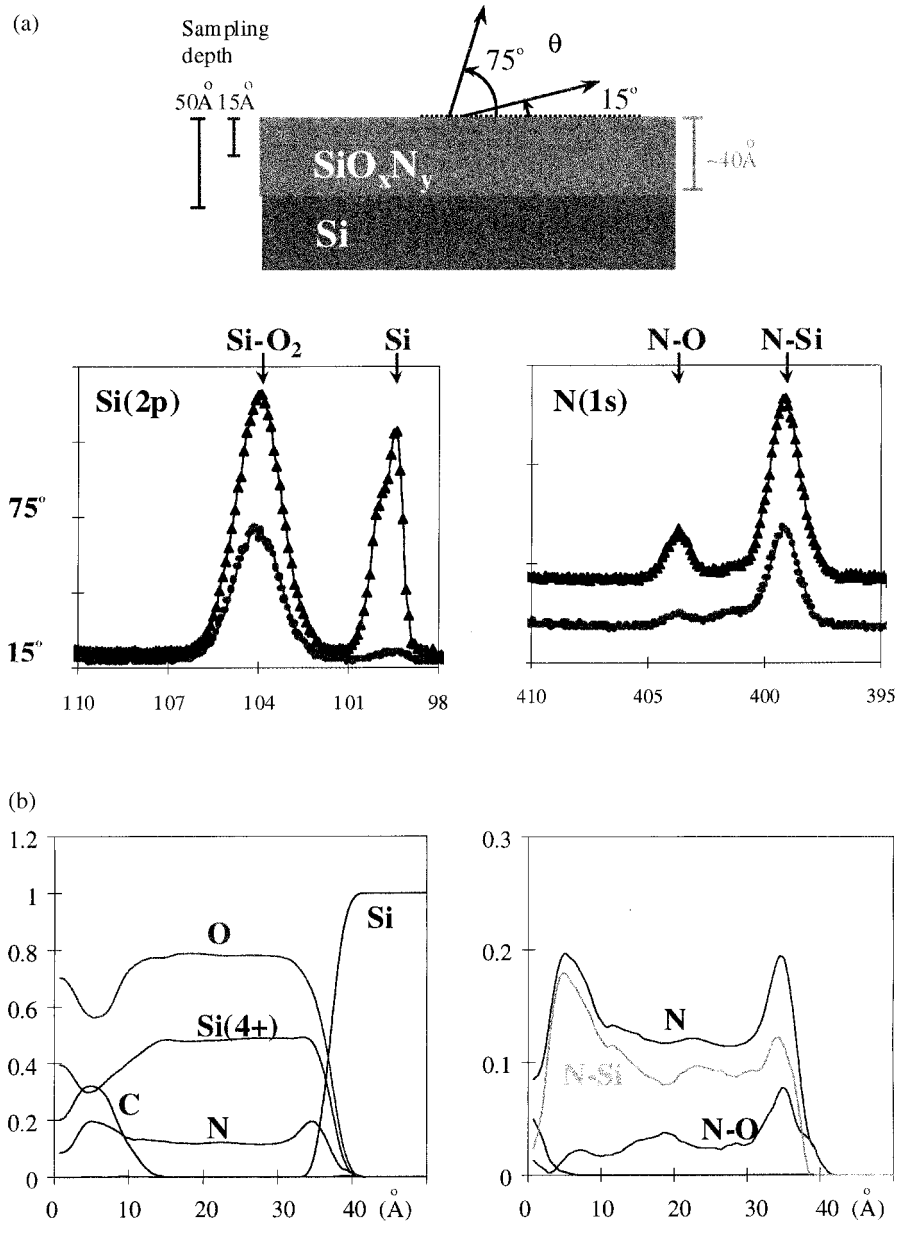

Fig. 14. (a) Depth profiling by XPS. Figure courtesy Jane Chang and Marty Green. (b) XPS depth profile of nitride/oxide/nitride dielectric. Figure courtesy of Jane Chang and Marty Green.

dies showing a densified oxide layer and the change in band gap for stressed oxide, this data is interpreted as meaning that the 1 nm thick interface consists of a sub-oxide layer with a densified structural transition layer on top [6]. *It should be noted that the methodology discussed above has just been introduced and a more extensive description of the model needs to be published and reviewed.*

Depth profiling in XPS is usually accomplished using sputtering or chemical etching methods. A non-destructive depth profile of thin films (< 10 nm) can be calculated from XPS spectra taken at different emission angles [35]. N depth profiles in nitride–oxide–nitride structures are an excellent method of determining N concentration and position when reference materials are available. In Fig. 14(a) and (b), we show XPS angle dependent spectra and the resultant depth profile obtained by Green et al. [39]. These data agree

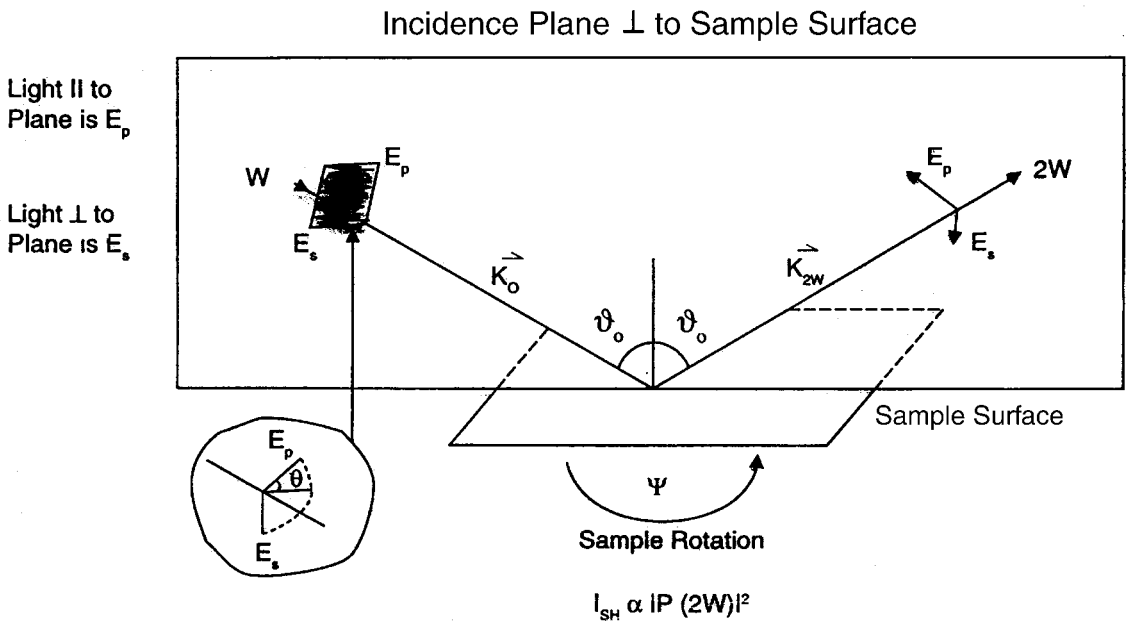

Fig. 15. Definition of s and p polarizations.

reasonably well with depth profiles determined by MEIS [32]. Opila has also studied nitrogen incorporation during nitridation [35]. This study showed that the N reacts and stays at the interface during N_20 anneal of a RTO oxide [35].

The oxide thickness has long been directly calculated from the relative intensities of Si 2p core level peaks [40]. The oxidized Si core emission in the overlayer is shifted from that of the substrate Si, thus allowing experimental determination of the ratio of photoemission intensity (I_{oxy}/I_{Si}) from these two Si 2p peaks. Photoelectrons leaving a solid are scattered as they leave a film and the probability for scattering scales linearly with the distance they must travel to exit through the surface. We quantify the scattering by using a photoelectron effective attenuation length, λ_{oxy}. The accuracy of the calculated oxide thickness depends on the accuracy of the attenuation length (current values for Si and SiO_2 are: 2.3 and 2.71 nm respectively for 1157eV Mg X-rays and 2.7 and 3.2 nm respectively for 1387 eV Al X-rays). The relationship for oxide thickness is:

$$d_{ox} = \lambda_{oxy} \sin \phi \, ln[I_{oxy}/(\beta I_{Si}) + 1],$$

where ϕ is the take off angle and β is the ratio (I_{oxy}/I_{Si}) measured on films thick enough to be opaque to photoelectrons. An XPS based determination of oxide thickness has also been compared to TEM, spectroscopic ellipsometry and capacitance–voltage measurements for films from 1.5 to 12.5 nm thick [40]. *This study indicated that electrical thickness values were slightly greater than physical thickness values and the physical measurements were in excellent agreement.*

3.2. Optical second harmonic generation

Optical second harmonic generation can be used to probe the interface between crystalline silicon and a transparent dielectric layer [41–48,106,107]. It has been used to probe the interface of $Si(111)/SiO_2$, $Si(001)/SiO_2$ and reconstructed Si(111) and (100) surfaces. The fact that OSG can observe the surface reconstruction effects on the surface symmetry means that OSG is sensitive to the monolayer thick crystal structures [48,107]. The second harmonic signal from Si(111) is much stronger than that from Si(001) and thus the high repetition rate of the titanium doped sapphire (Ti:sapphire) laser is required for study of Si(100) surfaces. In this section, the basics of OSG are presented along with a review of data described in the literature.

In OSG, the intensity of polarized light at twice the frequency of the polarized probe light is monitored as a crystal is rotated about the z-axis (axis perpendicular to the surface). The second harmonic output (i.e. the photons produced at twice the probe light frequency) is produced by nonlinear optical processes. The electric field of the light polarizes the electrons in the lattice. For centro-symmetric crystals such as silicon, the bulk polarization is very weak and only occurs in 'electric quadrupole' contributions [41]. However, the surface breaks this symmetry and the stronger surface dipole effect contributes to the observed signal. This is the

Table 1
Rotational dependence of optical second harmonic signal (for further information see Ref. [41] p. 1135)

Incoming/second harmonic polarizations	Isotropic polarization	Anisotropic polarization	Total functional dependence includes surface plus bulk polarization intensity $= \|P(2\omega)\|^2$	Rotational symmetry of total OS signal
Si(100)	surface dipole			
S s	0	0		
S p	const.	0		
P s	0	0		
P p	const	0		
Si(100)	bulk quadrupole			
S s	0	$b\sin(4\phi)$	$(b\sin(4\phi))^2$	8-fold
S p	constant	$b\cos(4\phi)$	$[a+b\cos(4\phi)]^2$	$A>b$ = 4-fold
P s	0	$b\sin(4\phi)$	$(b\sin(4\phi))^2$	8-fold
P p	constant	$b\cos(4\phi)$	$[a+b\cos(4\phi)]^2$	$A>b$ = 4-fold
Si(111)	surface dipole		total dominated by surface dipole	
S s	constant	$b\sin(3\phi)$		
S p	0	$b\cos(3\phi)$		
P s	constant	$b\sin(3\phi)$		
P p	0	$b\cos(3\phi)$		
Si(111)	bulk quadrupole			
S s	0	$b\cos(3\phi)$	$(b\sin(3\phi))^2$	
S p	constant	$b\cos(3\phi)$	$[a+b\cos(3\phi)]^2$	
P s	0	$b\sin(3\phi)$	$(b\sin(3\phi))^2$	
P p	constant	$b\sin(3\phi)$	$[a+b\cos(3\phi)]^2$	

reason OSG has surface sensitivity for silicon. For non-centro-symmetric crystals such as GaAs, the bulk is more easily polarized and bulk signal will be strong.

Interpretation of OSG requires a brief description of the terminology and selection rules. In Fig. 15, we show how the s and p polarizations are defined in respect to the crystal surface and probe light beam. In Table 1, we show the selection rules and the expected rotational dependance of the OS signal. The key points of this table are that the surface dipole for Si(001) only occurs for the sp and pp polarization combinations [41]. There is no rotational dependence to the surface dipole contribution. There is a rotational dependence to the weak bulk signal. The observed rotational dependence for the sp and pp polarizations occurs because the constant a in $[a+b\sin 4\psi]^2$ is larger than b resulting in a fourfold symmetry to these signals. This is in contrast to the Si(111) OS signal which has a rotational dependence to the surface dipole signal [41].

As mentioned above, OSG is not always sensitive to surface anisotropy. Another factor is the intensity differences expected from each polarization configuration. The data in Fig. 16 shows OS signal from the four possible polarization configurations. This data demonstrates how Table 1 can be used to judge the intensity of second harmonic signals according to the input and output polarizations for Si(100) [42,43]. The s-in /p-out and p-in/p-out polarizations result from the stronger surface dipole polarizations. Only the bulk quadrupole polarizations contribute to the s-in/s-out and p-in/s-out configurations and the signals are significantly weaker. Also note that OSG can characterize the surface of a crystalline substrate through an amorphous layer such as the nitride layer shown in Fig. 17. The high counting rates of the Ti-sapphire laser allow extraction of the signals from s-in/s-out and p-in/s-out configurations. This is also shown in Fig. 17. The first studies of the effect of surface roughness on OSG from Si(100) were done by Dadap et al. [42,43] and the results are shown in Figs. 18 and 19. This data was obtained using a Ti:sapphire laser operating at 800 nm with a repetition rate of 108 Hz. Since the p-in/p-out configuration has a contribution from the surface dipole, it was used to characterize the effect of microroughness on the OS signal. The intensity data was fit to $I_{PP}=h^2+[a_0+a_4\sin 4\psi]^2$, where h accounts for a constant (dc) offset due to isotropic contributions to the second harmonic signal [42]. As shown in Table 1, a_0 is due to the isotropic surface dipole and isotropic bulk quadrupole contributions while a_4 (listed as b in Table 1) is due to bulk quadrupole contributions. A plot of a_0/a_4 versus surface microroughness is shown in Fig. 20. If the OS signal is influenced by roughness at the Si/SiO_2 interface, then a_0/a_4 will not remain constant. In order to test for sensitivity, some of the sample had levels of microroughness that are considered to be large (RMS = 0.06– $\sim$ 0.4 nm) when compared to that expected for typical gate dielectric

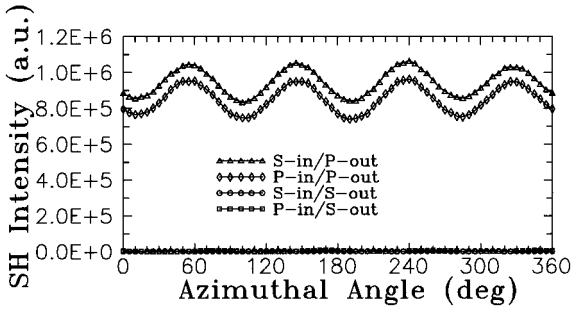

Fig. 16. Relative intensities of different combinations of incoming light and outgoing second harmonic polarizations. Figure first published in Ref. [42]. Reproduced with permission.

processes. Recently, Cundiff et al., have studied the effect of microroughness on OSG from vicinal Si(100) from 0 to 5° off axis in the ⟨110⟩ direction [44,106]. A series of samples with increasing oxide thickness was

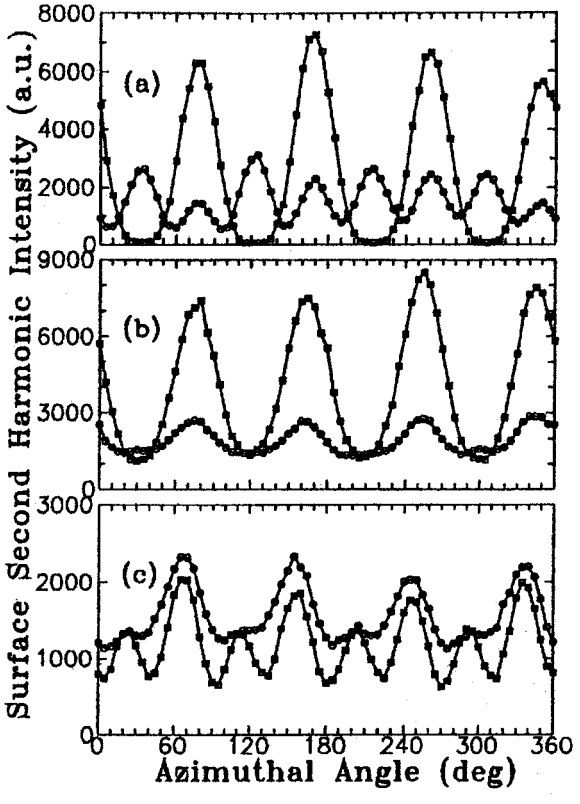

Fig. 17. The rotational symmetry of weaker s polarized second harmonic outputs. (This figure was first published in Ref. [43]. Reproduced with permission.) Circles = s incoming/s outgoing; squares = p incoming/s outgoing (a) silicon nitride on Si(100) (b) *n*-Si(100) (c) p-Si(100).

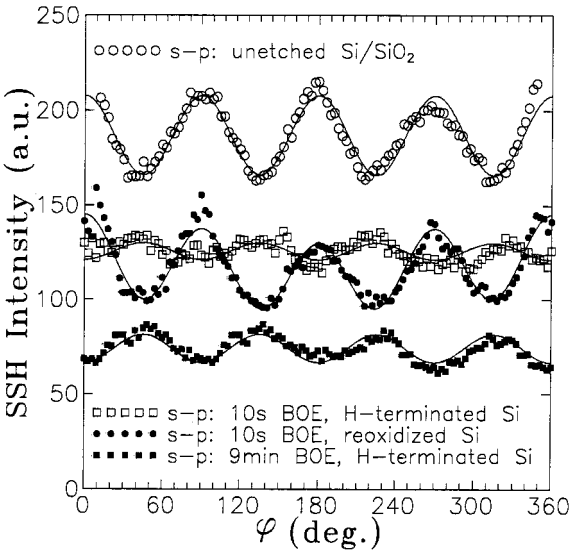

Fig. 18. Effect of surface microroughness on second harmonic signal. (Figure first published in Ref. [42]. Reproduced with permission.)

also studied. This work is in agreement with the conclusions of Dadap et al. [42,44,106].

Lucovsky has used OSG to determine the microscopic structure of Si(111) surfaces after hydrogen termination, oxidation, annealing and interface nitridation [45–47]. As discussed above, Si(111) surfaces have an anisotropic contribution to the surface dipole polarization for all input and output polarization configurations. This allowed use of a Nd:YLF laser at 1053 nm with a repetition rate of 10^3 Hz. Lucovsky and Aspnes have a new in situ chamber equipped with Ti:sapphire-based OSG. The Si(111) surface provides an interesting example of the sensitivity of OSG to surface structure.

A Si wafer cut ~4° off the (111) direction will have terrace structures. The expected rotational symmetry for a perfect Si(111) surface is listed in Table 1. The reason for the difference in expected response between sin function (see Ref. [41]) as shown in Table 1 and the cos dependence used in Ref [46] may be due to different definition of axes. Both have the 3ϕ rotational dependence. The surface dipole OS signal strength increases with off-axis angle for the s-in s-output configuration indicating that the electric field of the light can more easily polarize the offaxis surface [46]. The atoms at the step edges of the terraces on clean, oxide free surfaces have dangling bonds along the [49] crystallographic directions and contribute a signal that has the same symmetry as the atoms in the central part of the terraces. These same silicon atoms have bonds that can contribute to OSG when they are bonded to oxygen or nitrogen after oxidation or nitri-

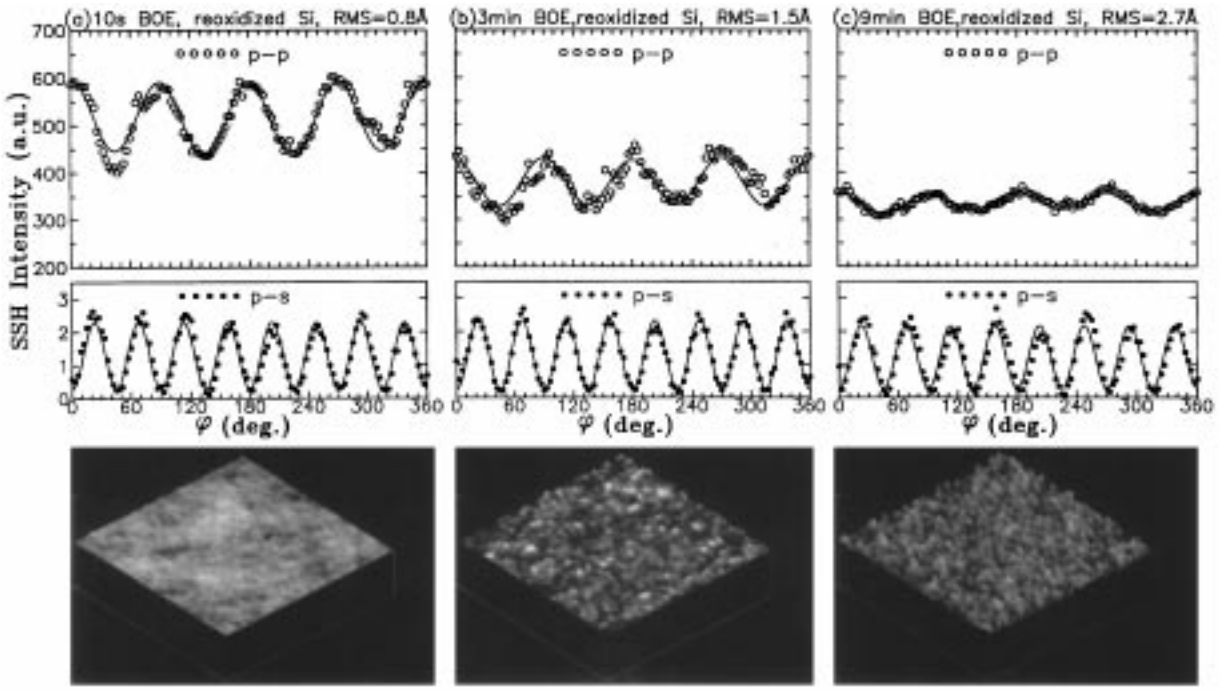

Fig. 19. Direct comparison of AFM and OSG. (Figure first published in Ref. [42]. Reproduced with permission.

dation of the oxide. Both have a cos(3ϕ) dependence to the polarization [46,47]. The steps are perpendicular to the ⟨1 1 2 bar⟩ direction and contribute a cos(ϕ) dependence to the polarization. Remember, the signal intensity is the square of the absolute value of the polarization. The relative phase between these two contributions is known to change with process conditions and second harmonic field has been represented by two different functional forms that are fit to the experimental data [46,47]:

$$P(2\omega) = A_1\, cos(\phi) + A_3\, cos(3\phi)e^{i\Theta} \quad \text{or}$$
$$P(2\omega) = A_1\, cos(\phi) + (a_3 + ib_3)cos(3\phi). \tag{1}$$

Changes in bonding energy effect the resonance energy for OSG which results in different OS intensities. Processing that results in oxidation of interfacial suboxides and reduction of oxide stress will also change the resonance energy. This changes the phase factors for the mixing of the cos contributions. In Table 2, we show the results of fitting these functional forms to OSG data from hydrogen terminated, remote plasma grown oxides on 3 and 5° off axis Si(111) and the effect of RTA temperature on these oxides [47]. In Fig. 21, we show how the ratio of a_3/A_3 fitting parameters relates to the midgap interface trap density of these oxides.

In Fig. 22 we show the results of OSG on clean, well ordered Si(l11)-2 × 1 and 7 × 7 surfaces in ultrahigh vacuum [46]. The change in rotational symmetry of these surface is due to the reconstruction of the Si surface atoms as dimers are formed. The (111) 2 × 1 and 7 × 7 surface structures of silicon are well understood through countless other surface structure studies.

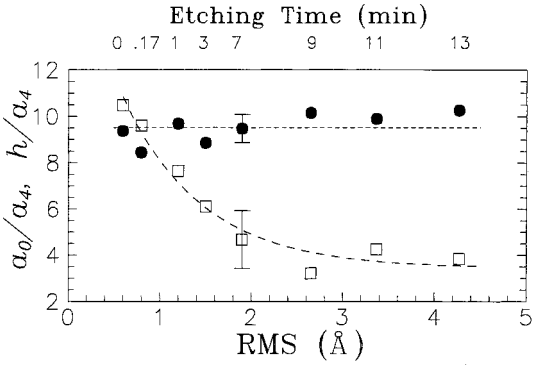

Fig. 20. Effect of surface microroughness on rotational symmetry parameters for {p in/p out}. (Figure first published in Ref. [42]. Reproduced with permission.) Open circles = a_0/a_4: filled circles h/a_4 $I_{pp} = h^2 + [a_0 + a_4 cos(4\phi)]^2$ h is the dc offset attributed to additional isotropic, noninterfering contributions to the SH signal.

Table 2
Effect of process conditions on phase relationship between terrace surface atoms and typical surface plain atoms to rotational anisotropy. Data from Ref. [47]

Sample	A_1	A_3	θ (°)	a_3	B_3	a_3/A_3
3°: RPECVD	0.17	0.62	72	0.19	0.59	0.31
5°: As-grown	0.41	0.59	73	0.17	0.57	0.29
3°: 950°C RTA	0.46	0.56	25	0.50	0.24	0.90
3°: 1000°C RTA	0.49	0.57	17	0.54	0.17	0.95
3°: H-terminated	0.1-1	0.26	154	−0.23	0.11	−0.90

3.3. Infrared spectroscopy

Infrared spectroscopy is a relevant tool to study thin oxides because it brings both chemical (stoichiometry, bonding configurations and impurity concentrations) and structural (homogeneity, stress, etc.) information. In principle, the Si–O stretching vibrations are sensitive to all the above factors. The problem, however, has been that the phonon spectrum of a thin amorphous oxide film is characterized by two broad and featureless bands, a transverse optical (TO) and a longitudinal optical (LO) band (which are polarized parallel and perpendicular to the plane of the film, respectively) from which it is hard to distinguish the various contributions and therefore to derive *unambiguous* information.

The observation of TO and LO optical transitions in noncrystalline media was first discussed by Berreman in 1963 [50], yet general acceptance of this interpretation was not gained for another 20 years. Indeed it was not until the work of Galeener and Lucovsky in 1976 [51,108] and de Leeuw and Thorpe in 1985 [52] that a consensus was finally reached. It is now widely accepted that TO and LO phonon modes can be observed in amorphous systems as well as it is in crystalline ionic materials. Just as in the crystalline case, coulombic interactions among the dipolar $Si^{\delta+}O^{\delta-}$ subunits leads to the splitting between the TO and LO phonons, with the LO mode frequency being related to that of TO by the generic equation [53]:

$$\nu(\mathrm{LO})^2 = \nu(\mathrm{TO})^2 + 2(\rho/\varepsilon_\infty)(e^{*2}/m(2m + M)), \qquad (2)$$

where ρ is the average density, e^* is the effective dynamic charge of the subunit, m and M are the atomic masses of O and Si in the subunit, respectively; ε_∞. is the average high frequency electronic dielectric function of the oxide film. As discussed below, the ρ/ε_∞ term, involving macroscopic quantities, describes all of the *physical*, i.e. 'spatial' and 'optical' information about the film; in contrast, the ν(TO) term, as well as the microscopic parameters (e^*, M and m), contain the chemical (i.e. structural/bonding) information.

Following the pioneering work of Berreman [50], Galeener and Lucovsky [51,108], Sen and Thorpe [54] and de Leeuw and Thorpe [52], the majority of the subsequent research has focused on developing an understanding of how macroscopic and microscopic physical and chemical phenomena influence the evolution of these phonon modes. In particular, a great deal of attention has been paid to the development of

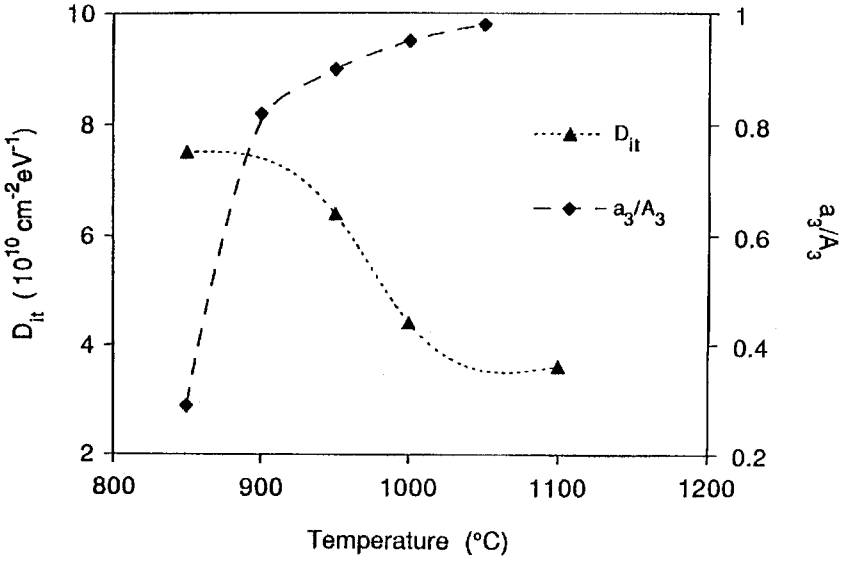

Fig. 21. Relationship between OSG measurements and electrically observed interface charge trapping states. (Figure first published in Ref. [47]. Reproduced with permission.)

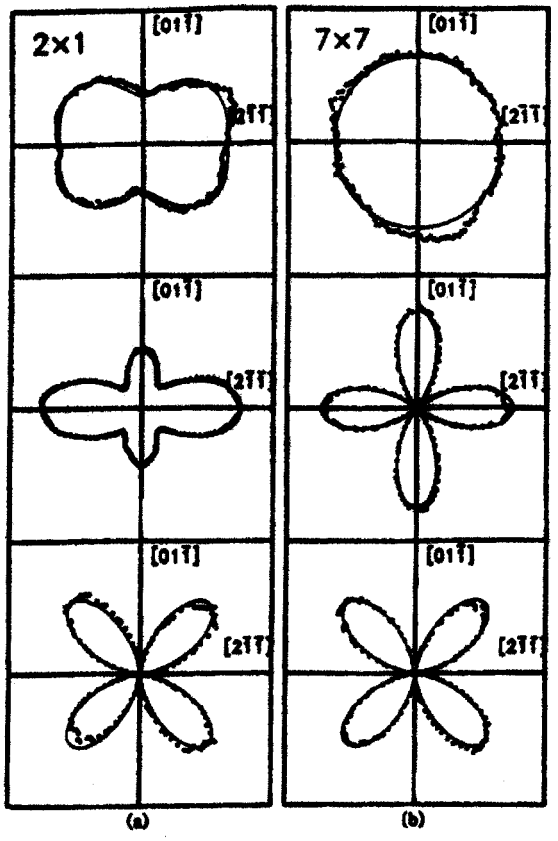

Fig. 22. Observation of surface reconstruction on clean Si(111) surfaces in ultrahigh vacuum by OSG. (Figure first published in Ref. [48,107]. Reproduced with permission.)

simple microscopic models of the constituent atomic motions at a pseudomolecular level. Models such as the Bethe Lattice, random bonding model (RBM) [55,109] have been coupled with the so-called central force model (CFM) [56], that utilizes the SiO bond stretching coordinate to describe the relevant interaction potential, or the related non-central force model (NCFM) [57], which includes both SiO stretching and bending. In this way the bonding and resultant vibrational spectra of glasses of stoichiometry AX_2, such as SiO_2 have been approximated. The specific details of each model will not be discussed herein: the essence is usually to reduce the problem to one of a single tetrahedron with a varying number of attached Si and O species at the periphery and to compute the associated vibrational modes by the CFM/NCFM relations [56,57]:

$$\nu(\mathrm{TO})^2 = 2/m[\alpha\, sin^2\, \theta/2 + \beta\, cos^2\, \theta/2], \quad (3)$$

where α is the central force constant, β is the non-central force constant and θ is the Si–O–Si bridging bond angle (see below). The majority of such phenomenological models reproduce the essential spectral features quite well, but typically have limited applicability when a comprehensive set of experimental spectra is considered. The essential problem is that the molecular-type vibrational modes are strongly mixed in an amorphous SiO_2 network and are broadened due to the relatively large variation in Si–O–Si bond angles ($\sim 140^\circ \pm 30^\circ$) that connect the tetrahedra, making the prediction of the extended mode spectrum difficult in the absence of a realistic model. Alternative approaches, based on empirically-derived potentials have also been investigated but the results of these methods vary widely and are generally found to reproduce the experimental spectrum only after significant refinements to the potentials are introduced.

In contrast to the above empirical models, Pasquarello and Car [58,110] have recently calculated the infrared absorption spectrum *from first principles* using density functional theory on a 72 atom SiO_2 slab. The model structure is based on corner-sharing tetrahedra that are quenched from the 'melt' using quantum molecular dynamics. A polarization theory based on quantum phase concepts was then utilized to derive the appropriate dynamical charge tensors. In this way, excellent agreement is obtained between the intensities *and* TO/LO peak positions (1065/1252 cm^{-1}, respectively) in the theoretical and experimental infrared spectra. In order to give some insight into the nature of the normal modes that give rise to the TO and LO modes, the total density of states was projected onto the tetrahedral symmetry group, T_d. The T_d group possesses an A_1 (totally symmetric) nondegenerate representation, which in this case describes the in-phase motion of all oxygen atoms towards the central Si, as well as a T_2 (asymmetric) threefold degenerate representation associated with the motion of two O's towards the central Si and two away (out-of-phase), with an opposing Si motion to keep the center of mass fixed. In this local mode description, it was found that the TO mode at 1065 cm^{-1} is due to the T_2 type motion, whereas the LO at 1252 cm^{-1} involves some of the A_1 motion in addition to T_2. Furthermore, the authors also explained the existence of additional features observed between 1150 and 1200 cm^{-1} — a low frequency shoulder on the LO mode at 1160 cm^{-1} and a high frequency shoulder on the TO mode at 1200 cm^{-1} — again in terms of a T_2 motion. These latter features have previously been attributed by Kirk [59] to a second LO/TO pair (at 1160/1200 cm^{-1}, respectively) that results from the out-of-phase combination of Si–O–Si motions that is infrared inactive (but strongly Raman active) for an ordered system, but becomes weakly active for disordered systems. It is therefore tempting to unify the *intra*tetrahedral mode description of Pasquarello and Car with the *inter*tetra-

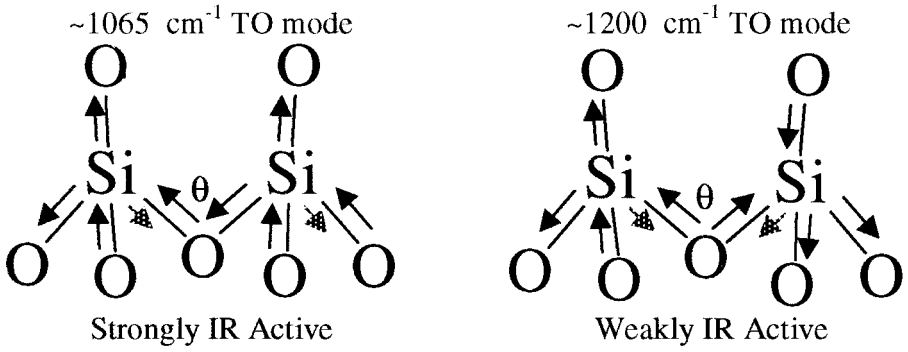

Fig. 23. TO vibrational modes of silicon dioxide. Unified picture of the *intra*tetrahedral mode description of Pasquarello and Car with the *inter*tetrahedral -Si–O–Si- bridging picture of Kirk.

hedral SiOSi bridging picture of Kirk to derive the following *schematic* picture of the relevant motions (Fig. 23):

It should be emphasized once again that any attempt to describe the extended phonon modes in terms of such local modes is fraught with ambiguity, nonetheless the above picture is consistent with the known literature. Specifically, in both cases the individual tetrahedra are executing a T_2 motion (as required by Pasquarello and Car [58,110]), with the difference between the low and high frequency motions being that the -O–Si–O- motions are in-phase and out-of-phase, respectively (as suggested by Kirk [59]).

Based on the preceding analysis, we should now be in a position to analyze how different physical and chemical phenomena influence the observed infrared spectrum of the oxide film. Unfortunately, one cannot rely on the first principles approach since the parameter space of interest is simply too large to allow accurate computation of the resultant spectra. Therefore, at present, the results of Pasquarello and Car [58,110] serve mainly to provide insight into the nature of the principal modes in the ideal 'pure' bulk case. The next-best approach is then to use the known optical constants for SiO_2 and SiO to model the infrared spectrum and then use Eqs. (2) and (3) to interpret deviations from these idealized results, as described in the following. Our discussion will focus on ultrathin oxide films (~30 Å or less) which are the principal interest of this review. However, the arguments presented above will generally also apply to all dielectric films of thicknesses (d) much less than the probing wavelength ($\lambda \approx 8$ μm).

We will start by considering the TO phonon mode(s). From Eq. (3) it is apparent that the frequency of the TO phonon depends on a number of factors such as the stoichiometry, the local stress and even the homogeneity of the oxide, as manifested in the value of the force constants α and β (see Eq. (2)) and the local Si–O–Si bond angle, θ. It is clear that if the constituent tetrahedra are oxygen deficient (i.e. the stoichiometry is SiO_x, where $x < 2$), a dramatic change in frequency will be observed due to the inclusion of non-SiO bonds. Such a loss of stoichiometry is expected at the Si/SO_2 interface, but can also exist in the oxide itself as result of defects and/or H incorporation. Similarly, local stresses in the film or at the Si/SiO_2 interface will influence θ and therefore the TO mode frequency.

What is less obvious, however, is that the TO frequency depends on the optical environment too. This dependence arises because the parallel component of absorption (i.e. TO function) is dependent on the imaginary part of the *average* film dielectric function, $\mathrm{Im}(\varepsilon)$. Consequently, spatial inhomogeneity of the oxide-involving media with different dielectric functions (i.e. density variations in SiO_2) will affects ε, which in turn will modify the observed TO absorption. It is important to recognize that, in fact, $\mathrm{Im}(\varepsilon)$ contains *all* the chemical and physical (optical) information about the film, so that if one could determine the complex dielectric function of a given layer, all the information regarding bond angles, stoichiometry and homogeneity/density variations would be contained therein. However, this is typically not possible as there are simply too many unknowns and too few experimental observables to allow separation into the individual contributions. Therefore, the favored approach is to describe ε as accurately as possible based on the known values for films with equilibrium bond angles and well-defined stoichiometries, so that the resultant 'ideal' spectrum can be calculated. It is then possible to use effective medium theory (EMT) [60,111] to convolute the known optical constants of one medium, e.g. SiO_2, with those of another component, e.g. Si, SiO or vacuum, to accurately deduce the spectrum of a film of mixed composition, as described below. In this way, the effect of inhomogeneities (such as those that result from interfacial roughness) can be assessed. It is important to realize that the resultant spectra contain

information regarding optical effects but no new chemical information (i.e. bond angles etc.), other than that supplied for the known (model) phases SiO_2/SiO. The relevant chemical information must be gleaned from the differences between the calculated and experimentally observed spectra, which can be interpreted in terms of Eqs. (2) and (3).

The LO mode frequency is also affected by all the above effects, as specified in Eq. (2). In addition, however, the values (or variations) of ρ, ε_∞ and e^* will contribute to further perturbations of the LO frequency above and beyond those due to intrinsic TO mode effects. Specifically, the density ρ, which might already have manifested itself in the TO mode behavior by producing changes in θ, will modify the LO frequency to a greater extent (physically, this is due to changes in the lattice sum that describes the spatial distribution of the constituent $Si^{\delta+}O^{\delta-}$ charges). The second influence on the LO mode frequency is the $(e^{*2}/\varepsilon_\infty)$ term which describes the magnitude of the screened charges and, combined with the lattice sum, defines the coulombic coupling intrinsic to the LO mode. Interestingly, both e^* and ε_∞ also influence the TO mode in the following way: e^* is known to be a sensitive function of Si–O–Si bond angle θ [56], whereas ε_∞ is the electronic part of the layer dielectric function ε, which defined the TO mode (as Im(ε)). At this point, it may seem that this interdependence of the TO and LO mode frequencies on these quantities precludes any simple analysis; however, the key point is that Eq. (1) requires that a different perturbation is produced for the TO and LO modes. Consequently, although a quantitative analysis is usually difficult, definitive *qualitative* statements can be made, *based on the different shifts observed for the TO and LO modes*. It is therefore *essential* to simultaneously study both modes by using appropriate experimental configurations. For further reading see Weldon et al. [61]

We will now consider a single experimental data set as an exemplary case for the changes observed in the TO and LO modes for ultrathin oxides, compared to the bulk SiO_2 case [61]. The data presented in Fig. 24 are for a thermal oxide film (grown at 800°C in O_2) as a function of thickness. The thickness variations were obtained by thinning several pieces of an oxidized wafer (initial oxide thickness = 31 Å) in very dilute HF (0.05% by volume), each piece for a different time [59].

It is clear from Fig. 24 that both modes shift continuously to lower frequency as the thickness decreases but, importantly, the LO mode exhibits a much more pronounced shift to lower frequencies (-44 cm^{-1}) than the TO mode (-14 cm^{-1}). These observations alone preclude or limit the role of a variety of the potential influences discussed above. On first inspection, these trends would seem to be consistent with the presence of stress-induced changes in the Si–O–Si bond angle,

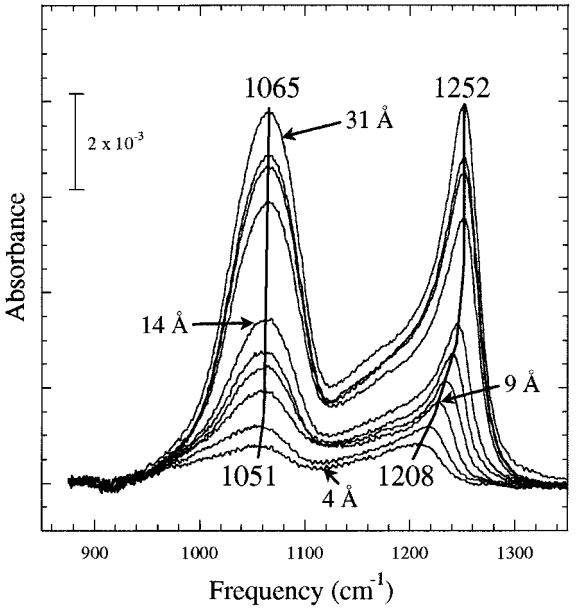

Fig. 24. Effect of thermal oxide thinning on TO and LO mode frequencies.

θ, since it is generally accepted that the SiO_2 at the Si interface is under compressive stress which, by Eq. (3), would produce a decrease in ν(TO) and a larger decrease in ν(LO). However, from the known angular (θ) dependence of e^* [58,110] it is straightforward to show that the TO–LO splitting cannot change by more than ~15 cm^{-1} by this mechanism, even for changes in θ as large as 20°. Indeed, if one uses the final TO frequency (1051 cm^{-1}) to estimate $\Delta\theta$ we find that only a 1 cm^{-1} difference in the TO and LO mode frequency shifts would be expected. Therefore, only a relatively small fraction of the observed shifts can be attributed to such stress-induced changes.

Next, one can estimate the effect of spatial inhomogeneities on the spectra using a Bruggeman effective medium treatment [60,62,111]. The effect of mixing 50% SiO_2 with 50% vacuum or silicon is shown in Fig. 25. The changes observed for the two are quite different: for Si the TO mode shifts to higher frequency by 20 cm^{-1}, whereas the LO mode shifts to lower frequency by ~20 cm^{-1} but is massively attenuated relative to the pure SiO_2 case. For the vacuum-SiO_2 mixed layer, the TO remains largely unchanged but the LO shifts down by ~20 cm^{-1} (without excessive attenuation). Clearly, neither mixture can explain the experimentally-observed trends. In contrast, a similar mixture of SiO_2 and SiO is found to qualitatively reproduce the observed changes, ν(TO) shifts by -15 cm^{-1}, whereas the LO is now comprised to two closely spaced peaks with a mean frequency of 1210 cm^{-1}, corresponding to a shift of -42 cm^{-1}. This agreement

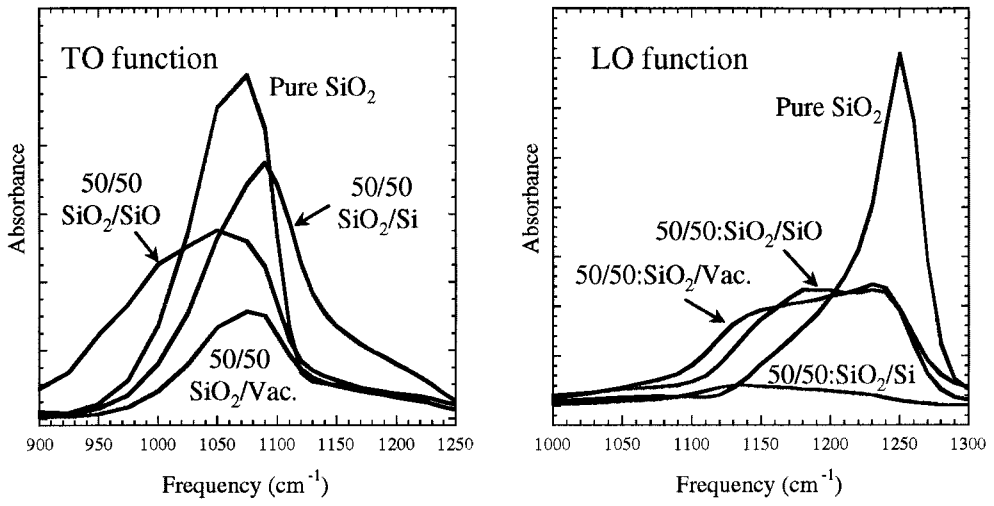

Fig. 25. Effect of interfacial roughness on TO and LO mode frequencies as modeled by Bruggeman effective medium treatment.

is remarkable, given that it is highly unlikely that Si–O type species are the only substoichiometric species present. Inclusion of species such as $SiO_{1.5}$ (which would correspond to the +3 Si oxidation state observed using XPS) would likely produce an additional LO peak at intermediate frequency, so that the net effect a single broad feature at ~1210 cm^{-1}, as required.

Considering all of the above, the most likely interpretation is that the principal spectral changes observed for ultrathin 5–10 Å oxide films, relative to the bulk case, are due to the presence of substoichiometric species at the Si/SiO_2 interface. This finding is in agreement with the recent work of Devine [63] for such thin thermal oxide films, based on studies of both the TO and LO mode shifts observed. The interfacial stress that is almost certainly present in these films is found to have only a relatively minor role. In contrast, previous workers have invoked interfacial stress as the *principal* origin of such changes, but such analyses are typically based on observation of either the LO [18,62,64] or TO mode [8], but not both simultaneously. It should be apparent from the preceding analysis that such incomplete data sets prevent definitive spectral interpretation.

A group at Hiroshima University has also reported [7] combined TO/LO measurements for chemically thinned thermal oxides (analogous to the experiment discussed above). Importantly, although the LO data were substantially similar to that in Fig. 24, the TO mode was observed to shift *up* in frequency with decreasing oxide thickness, causing the authors to interpret their results in terms of a combination of interfacial stress and microroughness. The differences in the two data sets point to differences in sample preparation, either in the oxide film growth itself (which would be of considerable interest) or in the effect of the subsequent chemical thinning (e.g. uniformity and cleanliness of etching). At this point, it appears that sample etching protocol may contribute to the discrepancies because the frequency dependence of the TO observed in Fig. 23 is altered if a *single* oxidized sample is etched repeatedly; that is, if the same sample is etched rather than using many different pieces of the oxidized wafer, with a different etch time applied to each (thus avoiding the possibility of recontamination of the sample affecting the subsequent etching). Clearly, more work is required to address this issue.

In conclusion, state-of-the-art in infrared spectroscopy, as applied to the study of ultrathin oxides, does provide essential *qualitative* information by careful analysis of the TO *and* LO mode behavior. Such analysis seems to confirm the findings of other experimental techniques that the ~5 Å of oxide at the Si/SiO_2 interface is comprised of substoichiometric oxide states and is consistent with some stress in the oxide near the interface. This result is complementary to the ellipsometric data which suggests that a rough and very thin layer (<2 Å rms) is comprised of Si and SiO_x [14–16]. As described above, the existence of such a layer would hardly contribute to the infrared spectrum because of the relatively minor amount of SiO_x and the correspondingly suppressed LO mode (due to the excess of Si) in that layer. Instead, the infrared spectrum is dominated by the *oxide* inhomogeneity (stoichiometric roughness) that extends several angstroms above the interface. Specifically, the Bruggemann model discussed above for a mixture of SiO_2 and SiO gives a significant shift in the infrared LO and TO modes, while hardly contributing to a measurable index change (probed by the ellipsometric

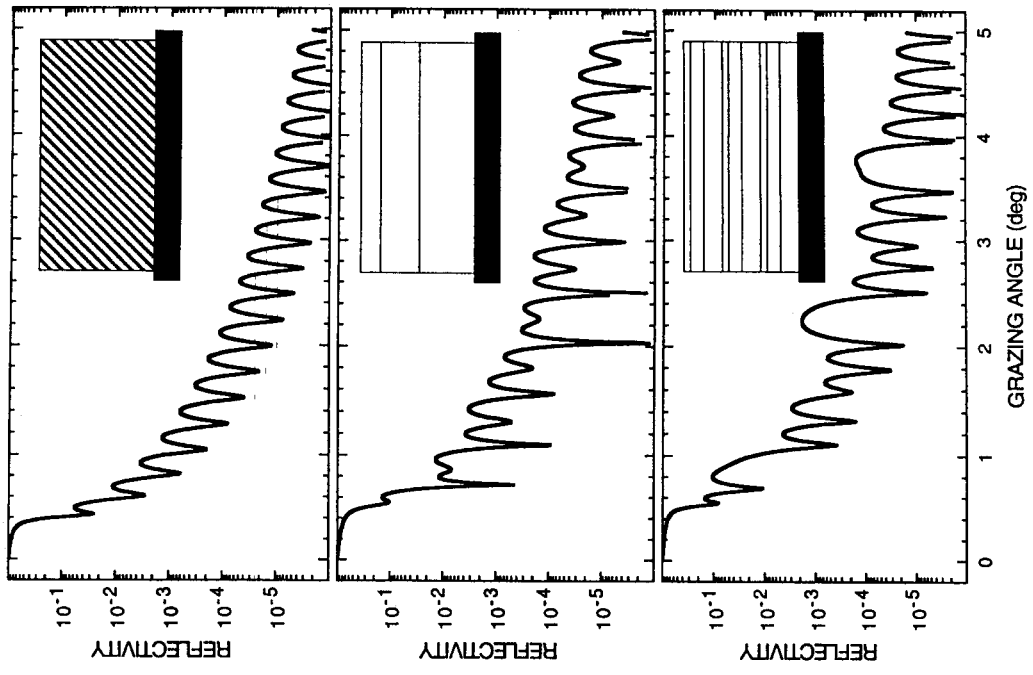

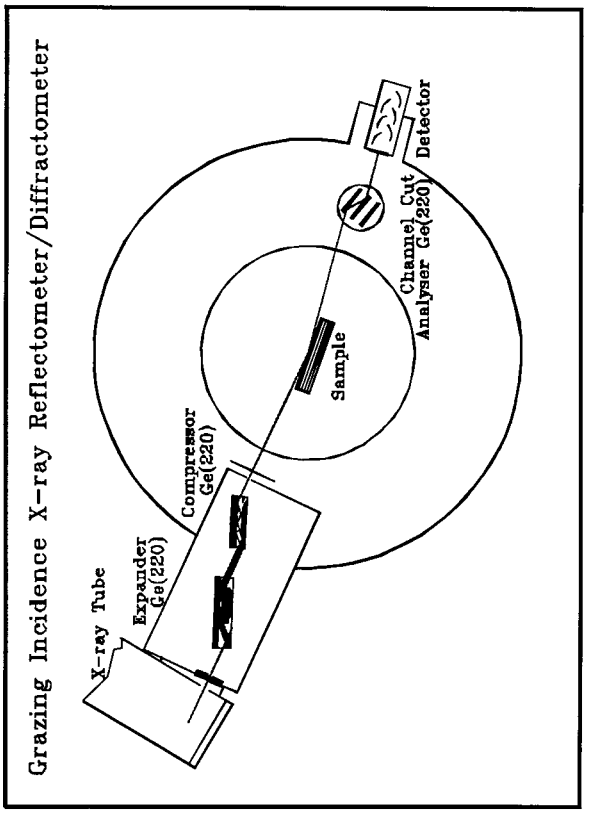

Fig. 26. Diagram of X-ray reflectivity apparatus. Figure provided by Richard Deslattes.

measurements). Conversely, a thin and rough layer of Si and SiO_x produces a large change in the dielectric function (i.e. in the ellipsometric response), while hardly contributing to the IR spectrum.

In addition to the complementary nature of infrared spectroscopy, it can also be applied in situ in a process environment and only requires ~1–2 min of data acquisition for acceptable signal-to-noise, using the latest generation of FT spectrometers. As such, armed with preceding analysis methodology, infrared spectroscopy could be used for optimization and/or quality control of oxidation processes. However, the ultimate goal must be to extend this work to attempt to uncover the *specific* bonding configurations present and to quantify their relative amounts. To achieve this goal, a combination of theoretical and experimental work is clearly required in order to characterize the different nonstoichiometric phonon states. Notably, recent combined infrared and theoretical analyses of step-by-step thermal oxidation reactions occurring under ultrahigh vacuum conditions [49,65] make it possible to assign specific parts of the IR spectrum to well-defined oxide structures, opening up the way for a better chemical characterization of the interfacial region. Such 'bottom-up' studies need to be coupled with further 'top-down' studies of actual, thin (5–10 Å) thermal oxide films produced in real process environments, before a definitive picture can emerge.

4. XRR and NR characterization of thin oxide films

In this section, we discuss measurements that provide an averaged view of a large area of the sample: XRR and neutron reflectivity. While ellipsometric measurements also average over the analyzed area, it is an accepted in-line metrology and we chose to describe it's status in the next section.

4.1. X-ray reflectivity

In XRR, the change in reflectivity of a well columnated, monochromatic X-ray beam is monitored as a function of angle of incidence [11,13,66–69]. The incident and exit angle are kept identical (specular scattering). When the angle of incidence is relatively shallow, X-ray penetration is minimized and thin films are more easily analyzed. In Fig. 26, we show a diagram of a typical XRR. apparatus [66].

One intermethod comparison criteria is the wavelength of the probe beam, but as we shall see, the wavelength differences between methods must be associated with the physical interaction between probe and sample and the model used to interpret the data. CuKα X-rays ($\lambda = 1.54$ Å) and 13 Å X-rays from a synchrotron source were used in the XRR studies of Refs. [10–11], respectively. The wavelength of light used in a single wavelength ellipsometer is 6328 Å. The wavelength of neutrons in NR is 4.75 Å [67,68]. Each of these methods interacts with the interface in a different manner and the fact that the X-rays have shortest wavelength does not necessarily make them the best probe for the thin interface layer. The phase information measured by ellipsometry provides a sensitive probe very thin layers. In addition, optical models usually consider the interfacial layer as a slab while one of the XRR and NR studies models the interface as an error function transition between two materials [67,68]. In this NR and XRR study, film thickness values represent the center to center distances of the two interfaces and the interfacial layer is actual a transition region between layers [67,68]. In two other XRR studies, the interfacial layer seems to have been modeled as a distinct layer with a higher density than the oxide or substrate. We save a more detailed method comparison for later.

X-ray reflectivity data are considered to be a Fourier transform of the spatial derivative of the sample density perpendicular to the surface, z. This density is averaged over the directions parallel to the surface (x,y) [11] and the data is displayed as a plot of $R(q)/R_{Si}(q)$ versus wave vector q [11]:

$$R(q)/R_{Si}(q) = \left| (1/\rho_{Si}[\mathrm{d}\rho(z)/\mathrm{d}z]\mathrm{e}^{iqz}\mathrm{d}z \right|.$$

XRR characterization of thin films on substrate layers is therefore sensitive to small density differences between layers: $(\rho_n/\rho_{Si})-1$ [11].

There have been three noteworthy XRR studies of the interfacial layer in thin thermal oxide layers grown on Si(100). [11–12]The results of these studies can be summarized briefly as follows. The XRR data was compared to three different models of the silicon–silicon dioxide system as follows: a single layer of SiO_2 at greater density than Si; a single layer of SiO_2 with less density than Si and an interfacial layer of greater density than Si between the substrate Si and SiO_2 with slightly less density than Si [11]. Silicon dioxide is expected to have slightly less density than Si. The model that uses an interfacial layer provides the best fit to the $R(q)/R_{Si}(q)$ data as shown in Fig. 27. Both studies observe an interfacial layer between Si and SiO_2 that has a greater density than either the Si or the bulk oxide above the interface. We summarize the density and thickness data in Table 3.

It is interesting to note that modeling the XRR data in both Refs. [11,12] requires use of an interfacial layer that is between 1 and 1.4 nm thick. This phenomenon is shown in Fig. 28. Awaji et al., studied the effect of annealing on the thickness of the interfacial layer of 4 and 7 nm thermal oxides. The thickness of the interfacial layer decreased while the density of the inter-

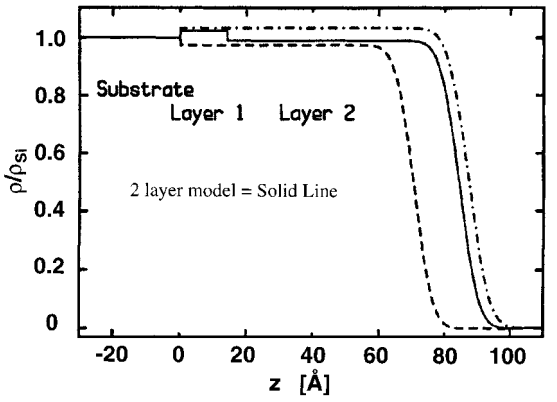

Fig. 27. Model used to interpret X-ray reflectivity data of thin oxide layers in Refs. [11,12]. A different model was used by the NIST group [68,69]. (Figure first published in Ref. [11]. Reproduced with permission.)

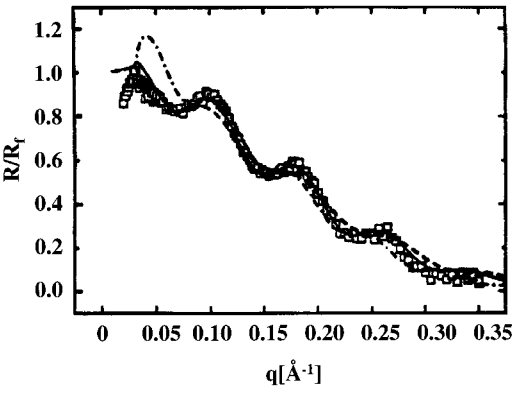

Fig. 28. Comparison of X-ray reflectivity data on thin oxide films to single layer and layer/interfacial models. Typical X-ray reflectivity data from an unannealed 7.5 nm oxide film. Also shown are the results for model based interpretation of the X-ray data. The fits with fits corresponding to the real space models of Fig. 27. The single oxide layer models (broken lines) produce poor fits, whereas the two-layer model (solid line) fits the data well. (Figure first published in Ref. [11]. Reproduced with permission.)

facial layer remained relatively constant. The data from Refs. [67–69] seem to be different from the other studies. When compared to the other XRR studies, the density of the oxide layer is lower and the interfacial layer thickness is less. However, the interfacial layer is considered to be the transition between layers of different density in Refs. [67–69] instead of as a separate layer as was used in Refs. [11,12]. Also, the ~0.2 nm interfacial layer thickness is comparable to that observed by other methods. It would be interesting to calculate the interfacial thickness for all the oxides using the both error function transition and a separate higher density layer between bulk oxide and bulk silicon. It is important to note that use of a surface contamination layer in the optical or X-ray model makes determination of a stack of three films difficult.

NR is considered by the authors of Refs. [67,68] to be a better method of characterizing Si/SiO_2 than XRR due to the higher 'scattering density' contrast. X-ray and electron 'scattering length density' increases monotonically with atomic number, while neutron scattering length can be large for light elements [67–70]. Scattering length density can be interpreted as the scattering cross-section multiplied by the density (electron density for X-rays and atomic density for neutrons). The model used to interpret the NRR data incorporates a surface contamination layer and error function transitions between layers. In this way, the interfacial properties that the NIST group determines by NRR and XRR can be compared. The results of this study show comparable interfacial thickness for NRR and XRR.

5. Ellipsometric and electrical measurement

In this section, we discuss film thickness measurements traditionally used for fab metrology of gate dielectrics. Ellipsometry and capacitance–voltage (C–V) measurements are described and the models used to interpret data are discussed and contrasted. Direct comparison of optical and C–V data requires improved models and the same physical phenomena must be accounted for by each method. For example, optical measurements based on models using an interfacial layer are not equivalent to the slab layer model

Table 3
Density and thickness of interfacial layer between Si and SiO_2 as measured by XRR

Surface contaminant (0.54 nm after clean)	SiO_2 optical thickness (nm) (density (gm/cm^3))			
	10 (Ref. [67,68])	7.3 (Ref. [12])	4 (Ref. [11])	3.3 (Ref. [12])
'Bulk' SiO_2	10.15/2.24	5.97/2.28	2.83/2.36	2.53/2.3
Interfacial SiO_2	0.18/???	1.47/2.37	1.21/2.41	0.96/2.36
Si substrate	NA/2.33	NA/2.33	NA/2.33	NA/2.33

of the oxide used in C–V interpretations. The material for this section was extracted from Ref. [71]. Tompkins has written an excellent reference on practical single wavelength ellipsometery [72] and a spectroscopic ellipsometry version of this reference has gone to press. Aspnes has written numerous papers covering everything from theory to equipment [73–75].

5.1. Multiwavelength and spectroscopic ellipsometers

In-line optical film thickness metrology is done using either single wavelength or spectroscopic (many wavelength) ellipsometers. The commercial single wavelength tools now use 4-single wavelengths chosen for optimal measurement of dielectric films typically used in IC manufacture based on silicon dioxide gate and aluminum metal–silicon dioxide interlevel dielectric processing. These systems use optics that simultaneously measure over a range of angles and focus to small spot sizes [76]. Multiple wavelength and spectroscopic measurements allow determination of thickness for unknown, multilayer samples, improve sensitivity to film thickness changes and improve data averaging [77]. The multiwavelength data from spectroscopic ellipsometers makes them very flexible in that they can be used to measure most new materials systems such as advanced high k gate and low k interconnect dielectrics. Measurement precision can be improved by averaging multiple wavelength or spectroscopic measurements. Despite this, 4-wavelength systems seem to have better precision when only 632.8 nm is used for gate dielectric thickness measurements. in single wavelength systems, one can calculate the thickness from Δ and Ψ and the problem of repeating values of Δ and Ψ after ~283.2 nm thickness due to the thin nature of gate dielectric films. Film thickness is determined in spectroscopic ellipsometers by fitting Δ and Ψ data taken at many wavelengths to a values calcu-

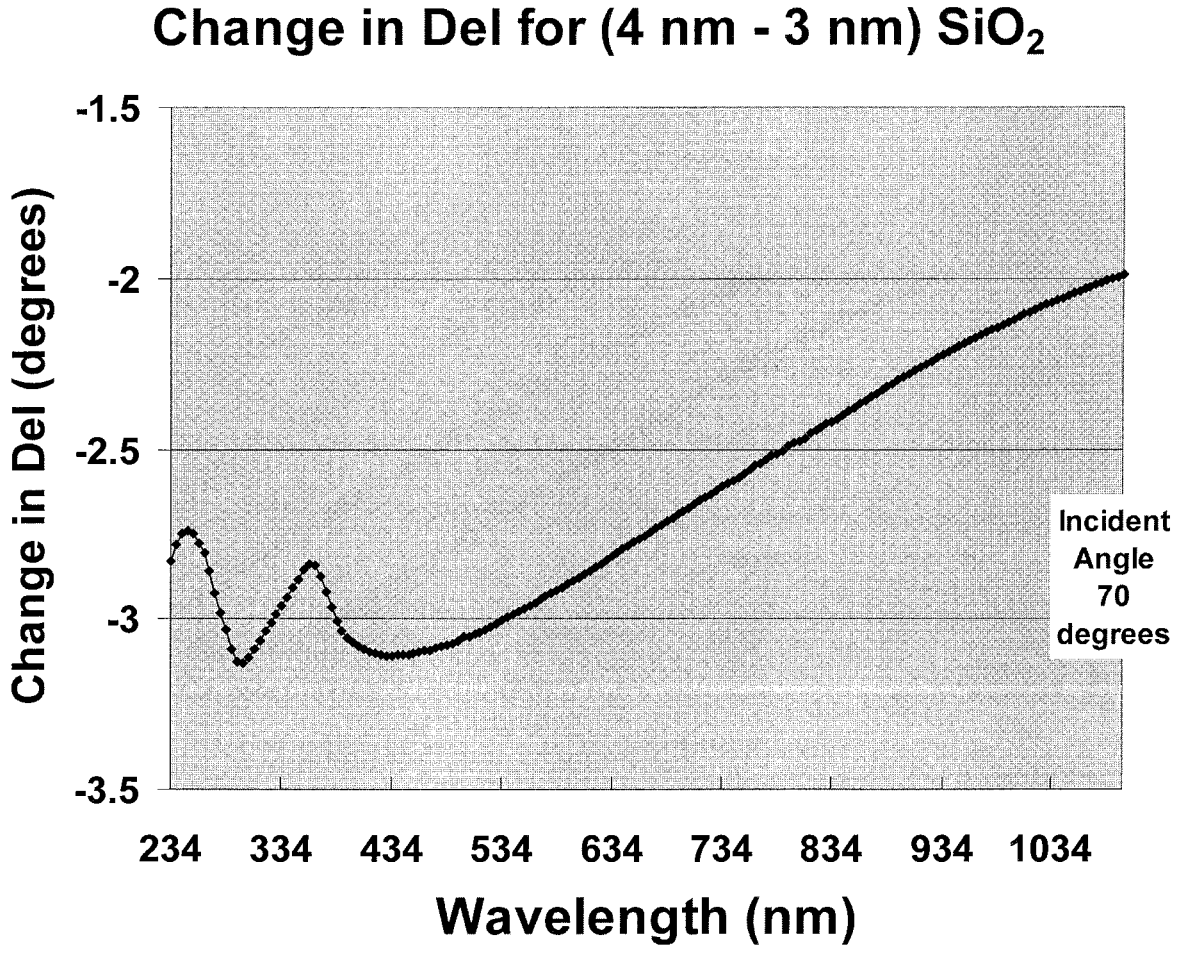

Fig. 29. (a–c) Change in ellipsometric parameters Δ (a) and Ψ (b) for 4 versus 3 nm oxide film calculated from a single layer. The effect of the angle of incidence (c). (Figure first published in Ref. [71]. Reproduced with permission.)

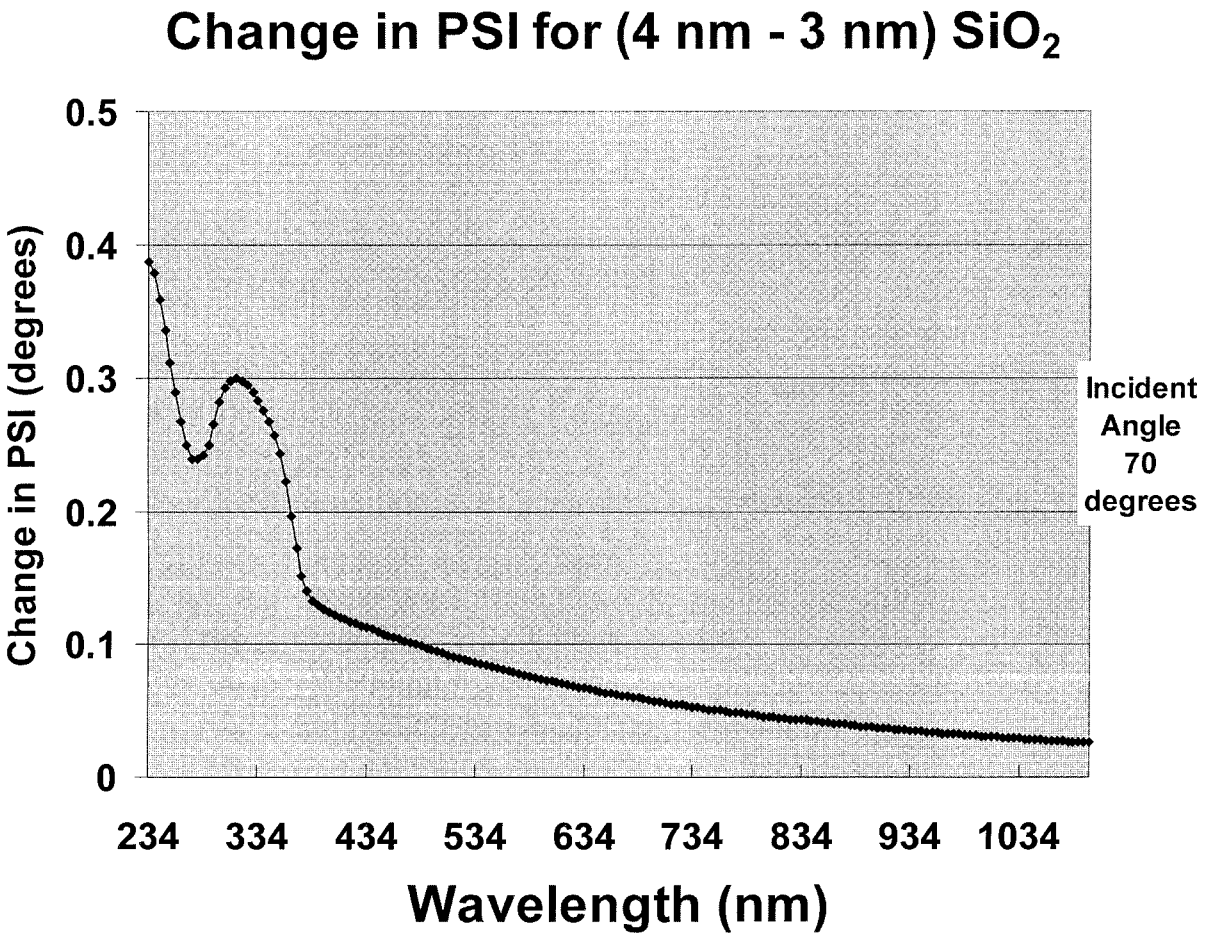

Fig. 29 (*continued*)

lated from an optical model of the sample. In Fig. 29a–c, we show plots of the change in Δ and Ψ versus wavelength from $\lambda = 234$ to about 1100 nm for a 4 versus a 3 nm SiO_2 film on Si. Fig. 29c shows that the sensitivity of ellipsometry to thickness change is a function of both angle and wavelength by plotting the change in Δ for the 4 versus 3 nm SiO_2 for 60–80° incident angle.

There are several different designs used for in-line ellipsometry. Block diagrams of multiwavelength and spectroscopic ellipsometers are shown in Fig. 30a–c. The rotating polarizer type ellipsometer depicted in Fig. 30a is typical of the design used in many commercial systems. There are a variety of system designs some of which incorporate a focus system that averages over a spread of angles as shown in Fig. 30(b) and (c). Precision requirements for ultrathin gate dielectric measurement may drive the use of nonfocused systems. Detailed technical descriptions of commercial ellipsometers are available from the technical literature [75–77].

5.2. Optical models of thin gate films

Ellipsometry measures the change in the state of polarization of light after reflecting from a sample surface. The polarization state is characterized by the ellipsometric parameters, Δ (del) and Ψ (psi), which describe the phase and amplitude change in the reflection coefficients of the polarized light. To measure the thickness of a film on a substrate requires the specification of an optical model of the system under investigation. The thickness is determined by iterative matching of Δ and Ψ calculated from the optical model, with the actual experimental data. The quality of the optical model and the uncertainty in the derived thickness is evaluated from the goodness-of-fit between the calculated and experimental data. The thickness, as

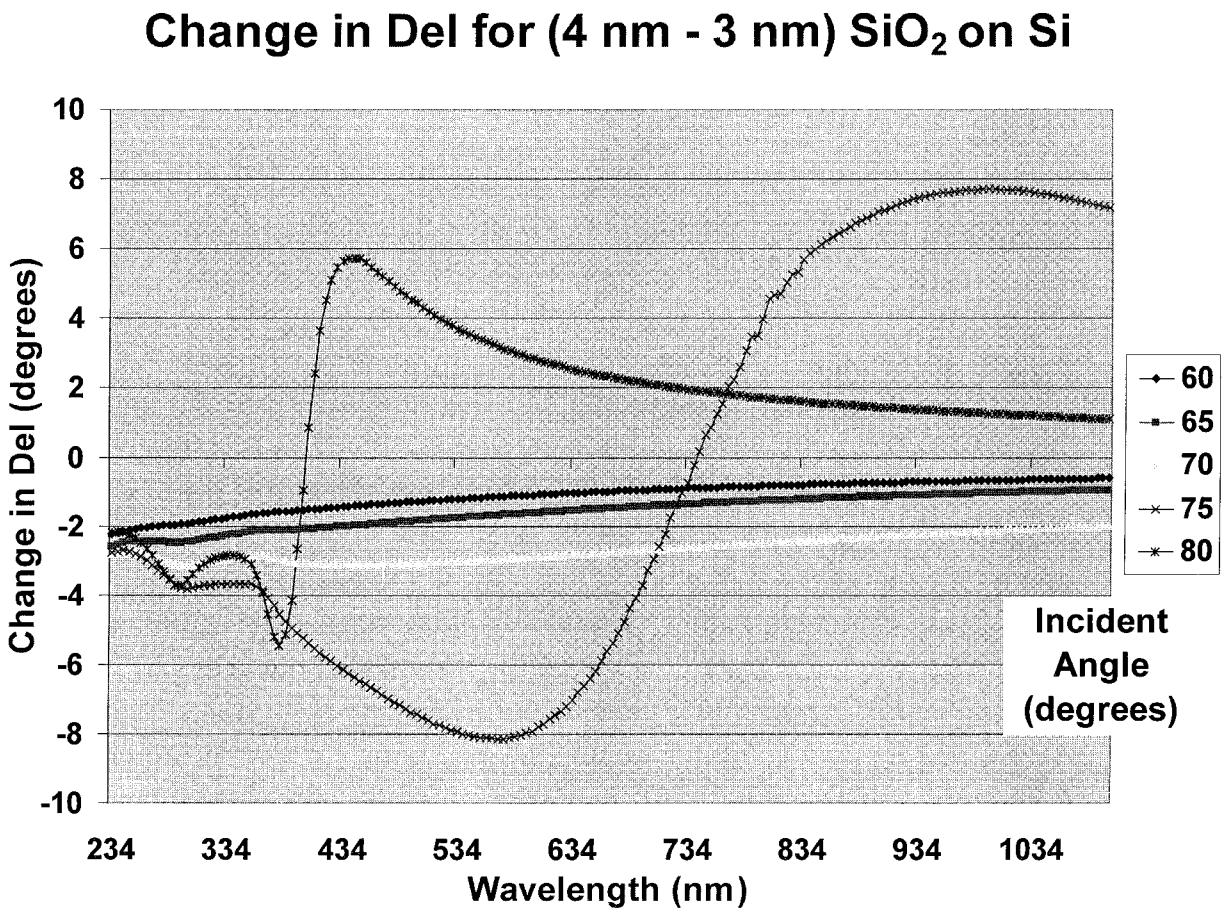

Fig. 29 (*continued*)

determined by such regression techniques, is only as good as the optical model chosen by the user.

Another important consideration for visible wavelength ellipsometry measurements done on very thin layers (<2 nm) is that the wavelength of light is much longer than path length change resulting from such a layer. Ellipsometry measures film properties over areas that are large enough to contain many local flatness deviations. The flatness deviations can be either terrace structures which are atomic in size or other deviations due to wafer fabrication processes [78]. An interfacial layer can be modeled as a slab that contains the silicon dioxide above and the silicon below the interface. Thus, microroughness is modeled as single layer of average dielectric constant formed from a mix of dielectric (optical) constants from the layer above and below the interface. In some instances, it is possible that the data for a two film stack fits an optical model that is insensitive to the ordering of the films. The pertinent example is a thin nitride/oxide film stack. In other words, characterization or process information is required to determine the true nature of the film (i.e. film a is on top).

The optical model consists of values for the refractive index (which is, in general, a complex number) of the film, the substrate and any possible interface layers, at each wavelength used in the measurements. For the SiO_2 on silicon system, the starting point for any modeling is the index of refraction for SiO_2 and for the crystalline silicon substrate. Bulk SiO_2 optical constants are usually based on Malitson's work on fused silica [79]. Bulk silicon optical constants are taken from various sources [80,81]. For many years it has been recognized that the optical constants of thermally grown SiO_2 on silicon are actually slightly higher than Malitson's fused silica values, apparently as a result of differences in density [79]. As a practical matter, these density differences have been incorporated into optical models in several ways. One method is to introduce a two-phase model consisting of Malitson's SiO_2 and voids. Typically, the best fit between experimental and calculated data is obtained with a small, negative void

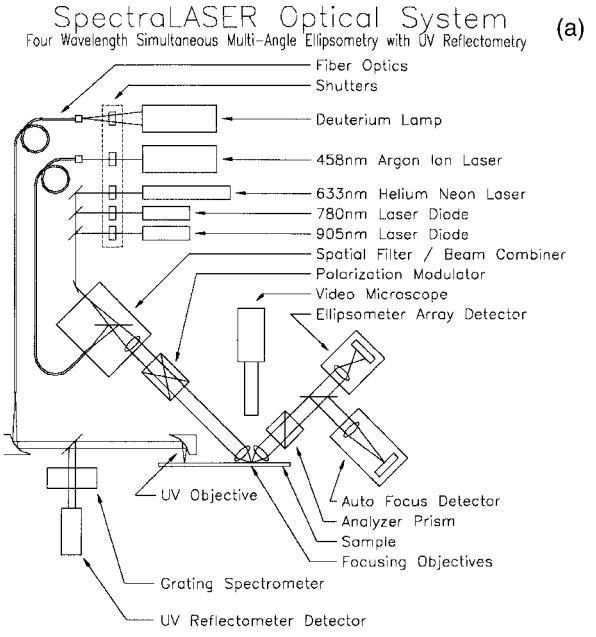

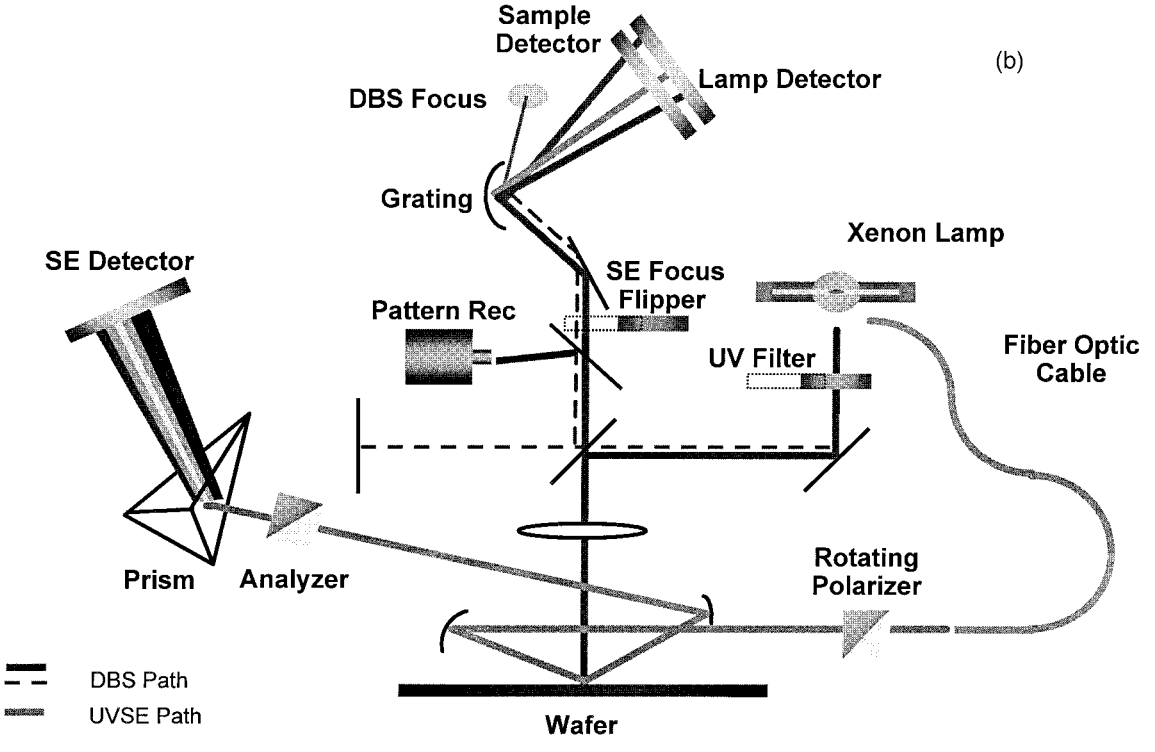

Fig. 30. (a–c) Block diagrams of three different commercial, in-line ellipsometers used for measurement of gate oxide thickness. (Figure first published in Ref. [71]. Reproduced with permission.) Fig. (a) provided by Rudolf Technologies, Inc; Fig. (b) provided by KLA-Tencor, Inc. and Fig. (c) provided by Thermawave, Inc.

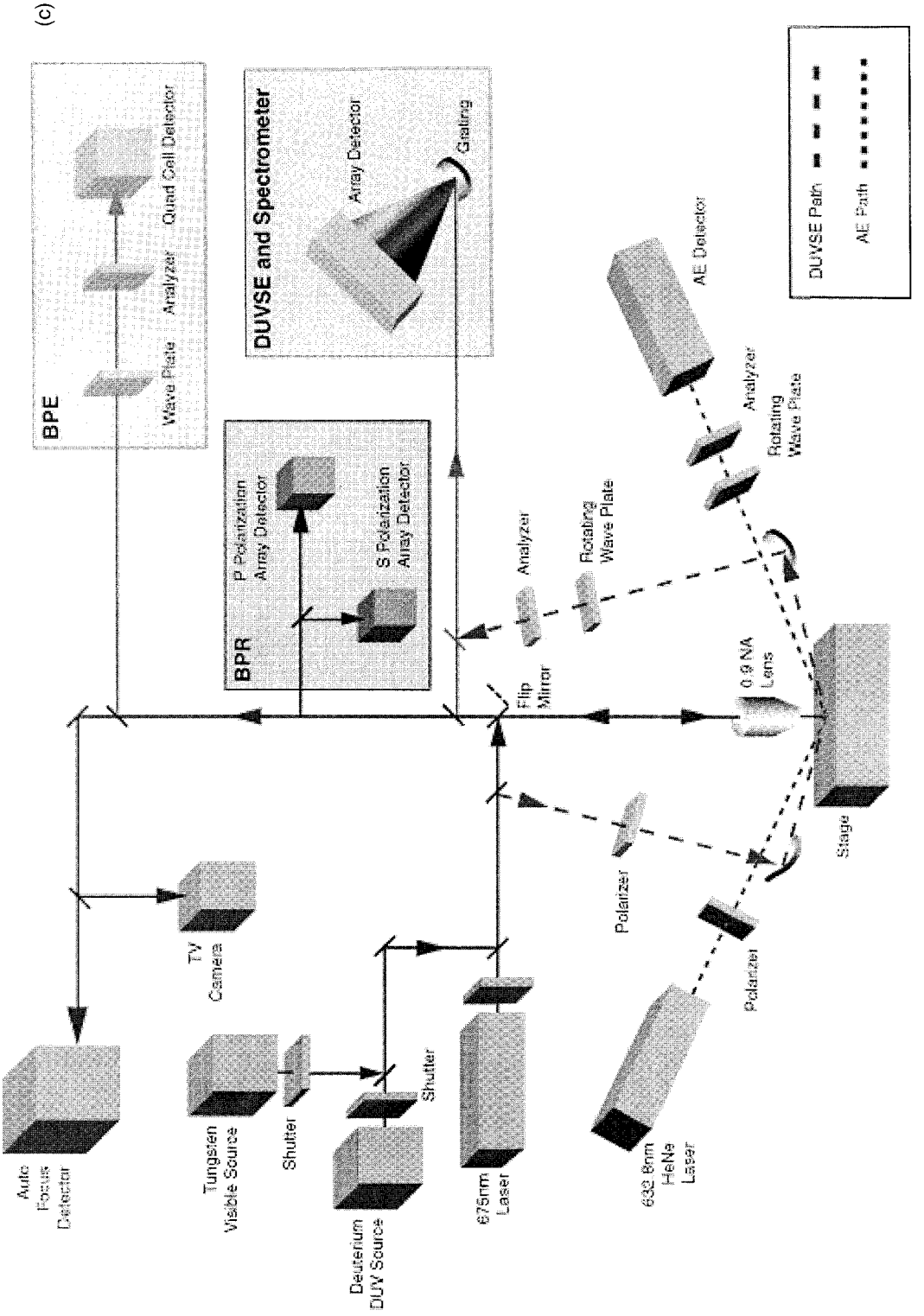

Fig. 30 (*continued*)

fraction [74,82]. Similar effects can be achieved by varying the offset parameter in Seillmeier representations [83] of the index of refraction for SiO_2 or by varying the oscillator number densities in harmonic oscillator models. Mixtures of amorphous silicon and $Si0_2$ have also been used [84]. Nayar et al. [85] have measured the optical constants of thermal oxide layers and the degree of the variability of the optical constants with process conditions remains an unresolved issue. The use of void fractions to model the optical constants of thermal oxides is a mathematical convenience and not an indication of the presence of voids in the oxide.

In addition to the apparent requirement that the index of refraction be slightly larger for thermal oxides, there exists abundant evidence that including an interface layer of intermediate refractive index between the silicon substrate and the oxide layer produces an improved goodness-of-fit. However, the precision with which the parameters in these interfacial models can be specified is rather poor. For example, Taft and Cordes [86] inferred the presence of a ~0.6-nm-thick interface layer of intermediate index of refraction from single-wavelength ellipsometry measurements of progressively etched back thermal oxides. However, they noted that their results were also consistent with interfacial layers of slightly different thickness and optical constants. Aspnes and Theeten [74,82] incorporated physical and chemical mixtures of silicon and silicon oxide to model this interface layer for thermal oxides characterized with spectroscopic ellipsometry. They concluded that the inclusion of almost any such mixture in the model improves the goodness-of-fit and that chemical mixtures produced somewhat better fits than physical mixtures. They report a best fit model consisting of ~0.7 nm of chemically mixed silicon (0.8 atomic fraction) and silicon dioxide (0.2 atomic fraction) with error bars of 0.2 nm on the thickness and 0.1 on the atomic fractions. Nguyen et al. [13] used a combination of single wavelength and spectroscopic ellipsometry to deduce the presence of a thin strained silicon layer beneath the oxide. Roughness at the interface between the silicon and the oxide film was modeled as a physical mixture of 88% silicon and 12% silicon dioxide. Helms' group found that between 70 and 90% Si [15] properly model the interfacial layer between thermal oxide and bulk silicon. The thickness of this effective layer was found to be 1.7 times the rms roughness of the surface as measured by a 1×1 μm using atomic force microscopy [15]. (N.B.: the rms roughness determined by AFM is determined over the range of surface wavelengths measured by AFM, down to a few nm [78]. Advances in probe tip technology will allow sampling of even shorter surface wavelengths.) Herzinger et al. [83] recently re-examined the interface issue in detail with variable angle spectroscopic ellipsometry measurements. They conclude that an interface layer in the sub-nanometer range with intermediate optical constants provides the best fit. However, they emphasize that correlation effects among the fit variables preclude an exact description of the nature of the interface layer.

It is important to recognize that almost all of the ellipsometric data included in these studies comes from fairly thick thermal oxides (typically greater than 10 nm) and that the data analysis includes measurements from multiple samples with varying thickness. For ultrathin oxides, in the thickness range 2–3 nm, the interfacial layer might constitute nearly a third of the entire film. However, parameter correlation effects, such as those noted by Herzinger et al. [83], become even stronger with such thin films. Moreover, multiple sample sets are incompatible with in-line metrology needs. Thus, it is unlikely that ellipsometry alone can provide an unambiguous analysis of the nature of the interfacial layer in the ultrathin thin film regime. As a result, it is almost certainly necessary to use the results of the various physical and chemical analysis techniques reviewed earlier to help specify a model for the interface in which there are no undetermined parameters.

5.3. Thickness resolution for ultrathin SiO and alternate dielectrics

First, it is instructive to evaluate the sensitivity of ellipsometry to changes in thickness of silicon dioxide. For a single wavelength ellipsometer using a laser operating at 632.8 nm, a change in thermal SiO_2 thickness of 0.1 nm results in a change in $\Delta \sim 0.25^\circ$ between 0 to 10 nm film thickness. Since the change in Ψ at a single wavelength is not a straight line function between 0 and 4 nm thickness, changes in Δ provide a better understanding of sensitivity to thickness changes [72]. A commercial ellipsometer is capable of measuring changes in Δ and Ψ of $< 0.01^\circ$. Several groups have discussed the sources of measurement error which effect accuracy and precision [13,14,87]. An error of 0.05° in incident angle near 70° results in a small error in Δ of $< 0.02^\circ$ and in Ψ of $\sim 0.1^\circ$ when $\lambda = 632.8$ nm [14]. Multiple wavelengths provides a method of averaging data that helps overcome errors.

Tompkins has used the Drude approximation to predict the linear change in Δ versus thickness for thin (< 10 nm), nonadsorbing (imaginary part of refractive index is small or zero) films of different refractive indices. The change in Δ at $\Psi = 632.8$ and 70° incident angle increases as refractive index increases [72]. The real part of the refractive index of silicon nitride and titanium dioxide is larger than that of SiO_2. Therefore, the resolution of ellipsometry to changes in the thickness of a single layer film of these materials on a sili-

con substrate would be better than for SiO_2. The refractive index of nonisotropic materials such as single crystal TiO_2 must be accounted for and an averaging procedure would provide the needed information for a film having randomly oriented grains. Since grain texture is process dependent, the optical constants of films made using new processes must be checked before using ellipsometry for process control.

Silicon nitrides and oxynitrides will probably be in manufacturing in the near future. The effect of small amounts of nitrogren less than 10% on refractive index is considered to be too small to be detected by most ellipsometry systems. However, some of the potential gate dielectrics are stacks of silicon nitride/silicon dioxide/silicon nitride. The nitride thickness in these stacks may be measurable by spectroscopic ellipsometry. Aspnes has described the modeling of silicon nitride's dielectric function [88].

5.4. Poly-Si thickness measurement

There is some interest in measuring the thickness of oxide layers under poly-silicon. Measurement of poly-thickness is difficult due to film variability [72]. The biggest issue is that the refractive index changes with microcrystallinity [72]. Although optical wavelength ellipsometry is hampered by the fact that silicon is adsorbant in this range, silicon is transparent in the infrared region. Recently, in-line ellipsometer systems have been equipped with infrared wavelength capability. It is also known that the microcrystallinity of poly-silicon or a-Si can change across a wafer. Poly-silicon and a-Si thickness measurement is routinely done with commercial systems after careful consideration of the above issues.

5.5. Electrical measurement of gate oxide thickness by C–V and I–V

This section briefly discusses the measurement of the effective dielectric thickness using capacitors or transistors. Comparison of optical and electrical measurements requires an understanding of the models used to interpret data and the sensitivity of each method to interfacial layers. Several references, which provide details of capacitance measurements, are recommended as supplementary reading [89–97]. In addition to these reviews, theoretical corrections have been used to extend capacitance measurements to 2 nm SiO_2 [95–98]. Again, the following discussion was first used in Ref. [71].

Capacitance–voltage measurement is used for much more than film thickness determination. C–V is sensitive to the effective dielectric thickness which is the thickness of the region that acts as a dielectric in the capacitor or transistor. The doped silicon and the oxide both collect charge [71,95]. Thus, the electrically measured thickness can be different from that measured optically when there is depletion of carriers in the poly-silicon above and/or in the silicon below the gate dielectric [71,95]. In Fig. 31a, a plot of capacitance versus voltage (called a C–V curve or plot) for an ideal capacitor illustrates the response of a SiO_2 film. Experience indicates that the ideal behavior is observed for thermal oxide films greater than 4 nm on a uniformly doped p-type substrate [89–97]. The assumption is that the poly-silicon gate and the uniformly doped p-type silicon both act as metal plates in a perfect capacitor when the applied voltage on the gate is negative. Band bending causes positive charge accumulation at the surface of the p-type silicon just as one expects positive charge buildup on a metal plate capacitor as illustrated in Fig. 31(b). The capacitance of PMOS structure drops as the voltage moves from negative toward zero. In a defect free structure the valence and conduction bands in the substrate are flat at an applied voltage equal to the flat band voltage. The flat band voltage for two 'metal' plates having the same work function is zero as discussed in the example shown in Ref. [92]. The equilibration of the Fermi levels (between the doped poly-silicon gate and uniformly doped substrate results in band bending at zero gate voltage and ideal flat band voltage $V_{fb}=(\phi_m-X_s-E_c+E_F)/q$. ϕ_m is the work function of the metal, X_s is the electron affinity of the doped silicon substrate, E_c is the conduction band edge of the doped silicon substrate, E_F is the Fermi level and q is the electric charge. A band diagram of the poly-silicon/SiO_2/p type Si system based on Ref. [94] is shown in Fig. 31(c) [92,94]. The C–V data is obtained by sweeping the voltage at either low or high frequency. This frequency has a large effect on the capacitance observed at positive voltage as shown in Fig. 31(a). Series and parallel capacitors have been used to describe the capacitance of the entire system as shown in Fig. 31(d) [93]. The capacitance of the oxide is in series with charge in the semiconductor and in the poly-silicon gate. The charge in the semiconductor is in parallel with the interface charge and Schroder divides the charge in the semiconductor into the hole accumulation charge 'C_p', the space-charge region bulk charge and the electron inversion charge which is not shown in Fig. 31(d) [93]. When the accumulated charge in the p-type silicon is very large and the 'C_p' is considered to be shorted and thus it acts as a perfect metal plate in an ideal MOS capacitor. For thicker oxides >4 nm, the gate electrode is considered to be a perfect metal capacitor plate. Using these assumptions, the effective thickness can be calculated using the following relationship, $C_{ox}=\varepsilon_{ox}A/d_{ox}$ [89–93]. C_{ox} is the maximum capacitance at negative applied gate voltage for PMOS, d is the effective dielectric thickness, A is the

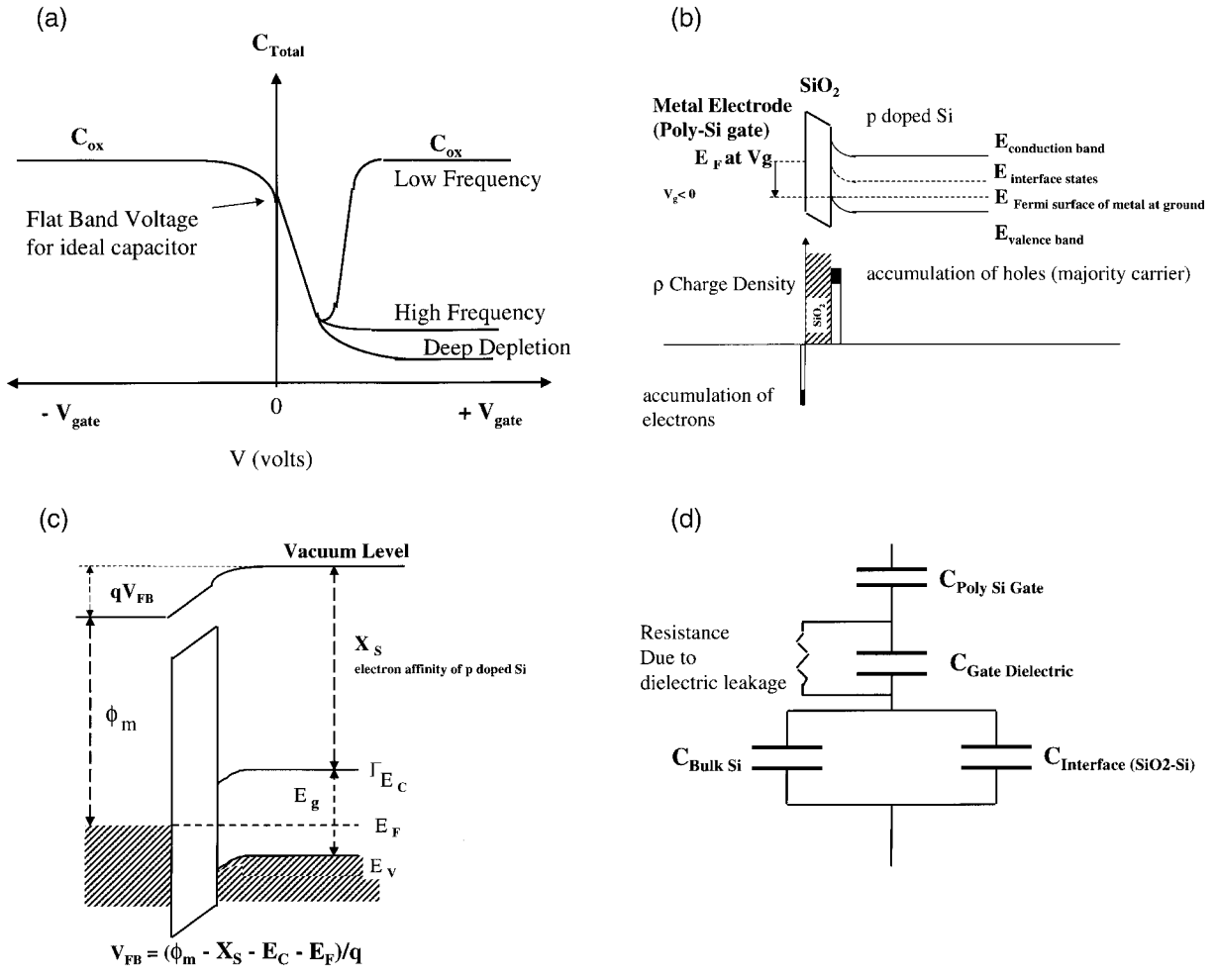

Fig. 31. Capacitance–voltage measurement of oxide thickness. Figure first published in Ref. [71]. Reproduced with permission. (a) Typical C–V data is shown. The oxide thickness is determined from the constant capacitance at negative voltage for p-type silicon substrates. (b) The band bending diagram and charge density plot for gate electrode and p-doped substrate show the charge accumulation at the p-substrate–gate oxide interface. (c) The origin of the flat band voltage. The energy band diagram for the polysilicon/gate oxide/p-doped substrate illustrates band bending at zero applied voltage. (d) The equivalent circuit diagram shows the various contributions to the capacitance of the transistor gate.

area of the capacitor and ε_{ox} is dielectric constant (real part of dielectric constant). Defects in the oxide layer result in the trapping of charge in the oxide layer [89–93]. This shifts the flat band voltage from its ideal value and allows the quality of the gate dielectric to be monitored by the value of the flat band voltage.

Several studies have shown an excellent correlation between C_{ox} and ellipsometric oxide thickness. By this we mean that a plot of the uncorrected electrical thickness versus physical thickness is linear. The electrical and physical measurements will both have contributions from the interface between the gate oxide and silicon substrate. The dielectric constant of the interfacial region is different from bulk SiO_2. This is not corrected for in the electrical determination of thickness. For the very thin oxides <4 nm, C–V behavior is not ideal, i.e. the capacitance is not constant in the accumulation or depletion regions of the C–V curve. The present status of correlation between electrical and physical measurements are discussed below.

Some workers have indicated that production FABs monitor oxide thickness on both uniformly doped substrates and on p-MOS and n-MOS test structures. This would be justified in one assumes that growth rate of SiO_2 is dependent on doping type (p versus n) and concentration especially for lightly doped regions. Therefore, the gate oxide (here we refer to >3 nm SiO_2) must be measured on test structures that have

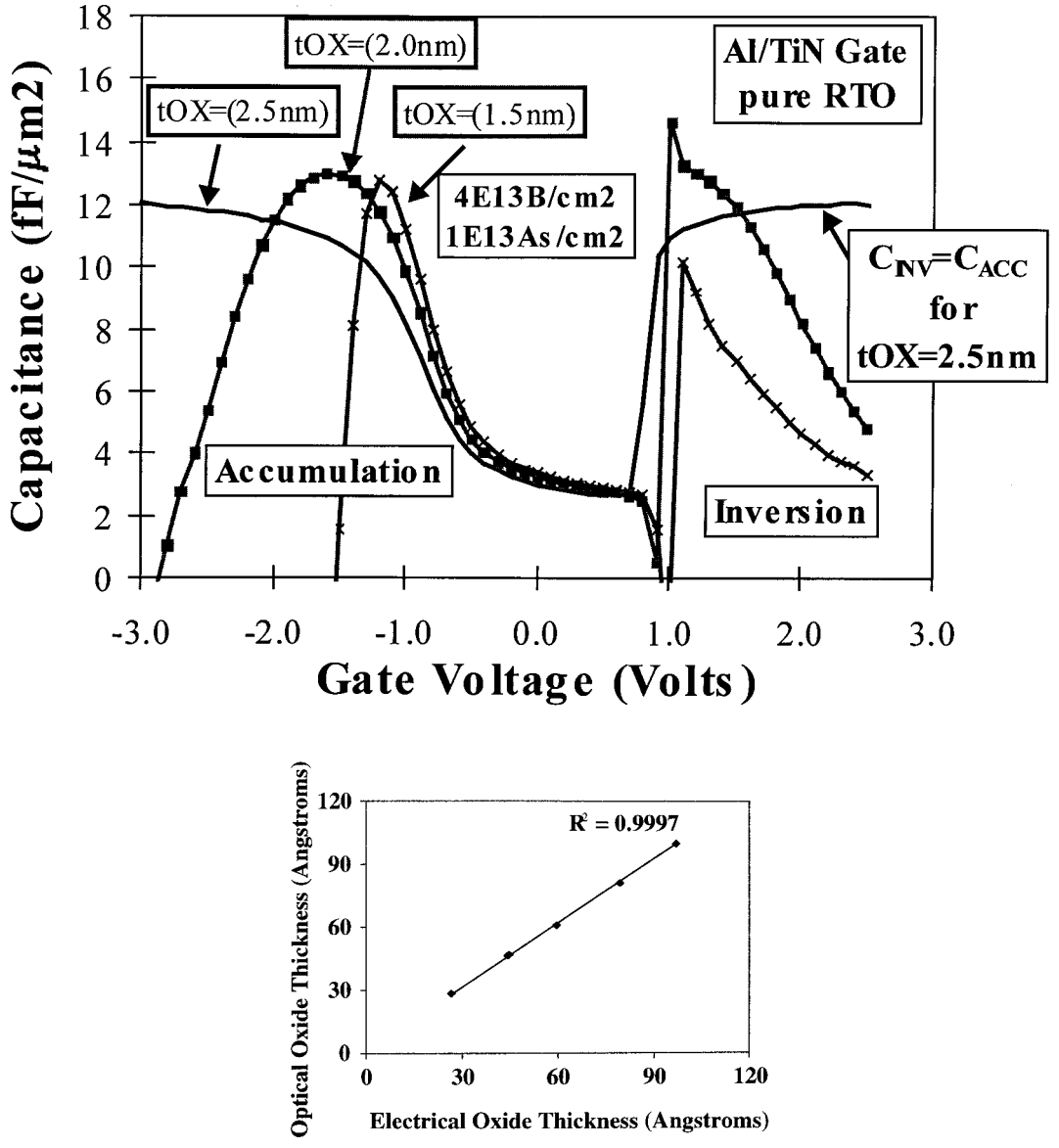

Fig. 32. Capacitance-voltage data for thin oxides using Al/TiN gate electrodes. All data is courtesy of George Brown, Texas Instrument. (a) *C–V* data for 2.5, 2.0 and 1.5 nm oxides made using rapid thermal oxidation show the increased non-ideal capacitance in accumulation and depletion as the oxide becomes thinner. (b) Correlation of *C–V* and single wavelength ellipsometry measurements.

implants representative of the channel region of a transistor. This means that when tight control of oxide thickness is required, the oxide thickness in both the channel in the PMOS and in the NMOS regions must be measured. The assumptions made in the evaluation of the perfect MOS capacitor, such as uniform doping, are no longer valid. The interface between the silicon and the 'bulk like' dielectric contributes to the measured capacitance. When this non-bulk oxide capacitance is constant or linearly varies with oxide thickness, correlation with optical (ellipsometric) measurement is possible. It is important to note that many manufacturing facilities only monitor a single type of test structure and do not subscribe to the need to monitor both p-MOS and n-MOS.

Depletion of charge in the poly-silicon gate and quantum states in the bent bands at the interface of the crystalline silicon with the gate dielectric layer alter the *C–V* behavior described above [71,95–98]. In Fig. 32(a), we show the *C–V* data for thermally grown SiO_2

ranging in thickness from 2.5 to 1.5 nm [99]. The 2.5 nm oxide has classical C–V behavior while 1.5 and 2 nm oxides show the effect of quantum behavior and poly-depletion. In Fig. 32(b), we show data demonstrating the correlation between C–V and optical oxide thickness measurements for thickness >3 nm. Several procedures for removing both quantum and depletion effects from C–V data have been described [95–98]. The resulting oxide thickness can be directly compared to ellipsometric measurements for the single (slab) layer model of the oxide with no interfacial layer. When the oxide is very thin, the voltage applied to the poly-silicon gate drops inside the poly-silicon gate electrode. This effect is a function of oxide thickness and poly-silicon doping. Modeling of the poly-depletion effect has shown that for a 3.5 nm oxide the ratio of measured gate capacitance to true oxide capacitance is about 0.84 for a poly-gate doping level of 2×10^{20} and ~ 0.75 for 5×10^{19} [95]. For a 1.5 nm gate oxide the capacitance ratios are 0.7 and ~ 0.55 for these gate doping levels [95]. Band bending at the silicon substrate–gate oxide interface allows the formation of quantum levels. When a negative voltage is applied and electrons are drawn toward the silicon substrate–gate dielectric interface, the accumulated electrons fill these quantum levels. The filled quantum levels increase the amount of band bending and cause the center of the accumulated charge to shift away from the interface. These effects change capacitance significantly and must be accounted for during electrical measurement of oxide thickness. In Fig. 33, the origin of the quantum effect is shown along with a theoretical C–V plot that is corrected for poly-depletion and quantum effects for a uniformly doped substrate. Fig. 34 shows both corrected and uncorrected theoretical C–V plots for a sub 3 nm SiO_2 gate oxide.

Measurement of very thin SiO_2 with most test equipment requires the use of high frequency ($\sim$1 MHz) and transistor structures that have a large width to gate length ratio [95,98]. Direct tunneling through thin oxides distorts the C–V measurement which can be avoided by use of high frequency (nonstatic) C–V. Static C–V measurement can be extended to $<\sim 2.5$ nm SiO_2 by use of special leakage compensation circuitry and numerical correction [98]. C–V metrology should be used for gate thickness on uniformly doped substrates. Simulation of C–V data for channel doped structures is not available at this time.

Recently, a new method of obtaining non-contact, C–V like data called the 'Quantox®' has been introduced. This tool can provide oxide thickness, flat band voltage and carrier lifetime data [100]. A corona charge, Q, makes the top "gate" for the capacitance measurements and provides the bias sweep. The Kelvin probe measures the surface voltage at each Q bias point and the surface photovoltage is the transient surface voltage measured at each Q bias point when a light is flashed to photoflatten the bands. This results in a low frequency non-contact Q–V–SPV curve. This is shown in Fig. 35. The author notes that there are differences between traditional C–V and 'Quantox®' measurements. The rate of voltage sweep is different from traditional C–V measurements and the amount of tunneling of current during Q–V–SPV measurement is considerably less. By pulsing the corona charge to deep deplete the silicon from inversion, non-contact measurements of carrier density and generation lifetime to a controlled depth are also provided. Existing data shows that repeatability is 0.03 nm, 1 σ. Some workers believe that Quantox measurements are not effected by hydrocarbon buildup on the oxide surface. In addition, poly-depletion corrections are not required.

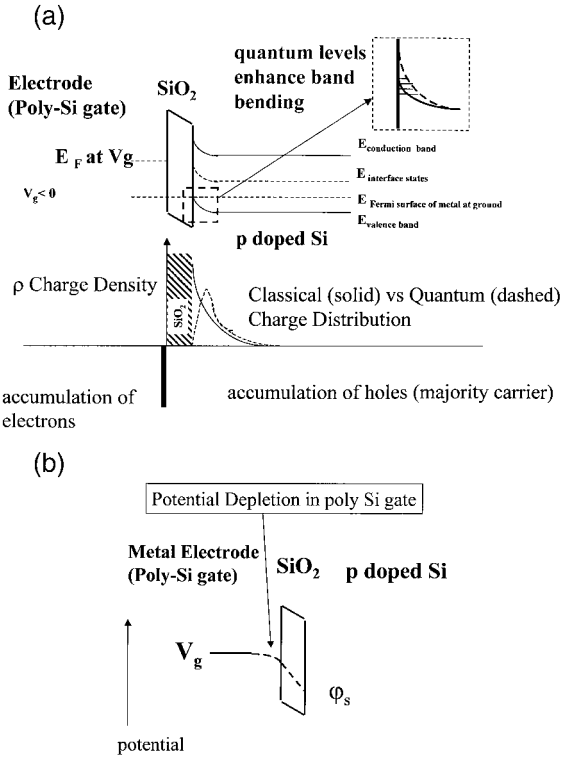

Fig. 33. Origin of the quantum mechanical and poly-depletion effects in C–V measurements. This figure shows the changes in the potential diagram of Fig. 31(b) and (d) due to depletion of charge in the poly-silicon gate electrode and quantum state induced band bending. The potential diagram is shown for a p doped substrate in the accumulation part of a C–V measurement. Although the poly-silicon is highly doped, it is not truly metallic and the potential starts to drop before the interface between the electrode and gate dielectric. The additional band bending results in a shift of the charge center of the electrons accumulated at the interface.

Current–voltage measurements also show a strong correlation to oxide thickness and may have better res-

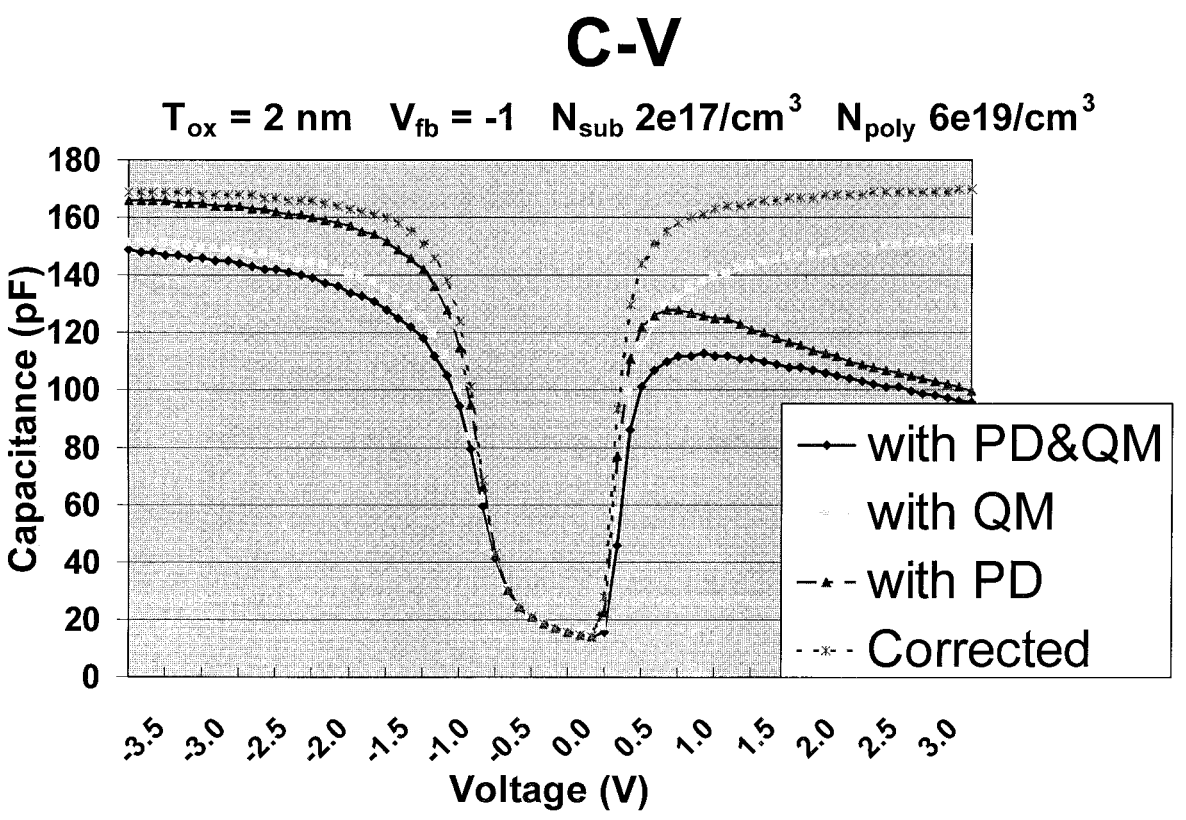

Fig. 34. Theoretical *C–V* simulation showing quantum and depletion effects. (Figure first published in Ref. [71]. Reproduced with permission.)

olution to changes in oxide thickness than ellipsometry [96,97]. Typical current voltage data is shown for oxide thickness' between ~3 and ~1.5 nm in Fig. 36. In Fig. 37, the current at 1 V is plotted versus the oxide thickness these same samples [99]. Since the *I–V* data is a strong function of oxide thickness (10 A/cm for a 0.04 nm decrease in oxide thickness), measurement resolution appears better than the approximate 0.25° change in Δ Å estimated for ellipsometry at 632.8 nm. On the basis of the measurement procedure reported by Brown et al., the thickness associated with measured current must be calibrated using another measurement. The *I–V* characteristics should depend on doping characteristics such as channel dose. Unless calibrated to *C–V*, *I–V* thickness does not depend on knowledge of the static dielectric constant. The thickness of thin dielectric layers can be determined directly from modeling [96–97]. The accuracy of model based thickness determination seems to be controversial.

5.6. Comments on direct comparison of optical and C–V measurements

As discussed above, optical thickness is calculated from the refractive index of the oxide film and those of the interface and substrate layers while a capacitance based thickness is calculated from the dielectric constant of the oxide film. Fundamentally, the two approaches should give the same value of the oxide thickness when both are interpreted using physically correct models. The complex refractive index is the square root of the frequency dependent dielectric function $\varepsilon(\omega)$ [101]. Although both quantities are complex numbers, low frequency electrical measurements of silicon dioxide thickness use the real part of the dielectric constant [93,94,101]. Dielectrics with large values of the imaginary part of the dielectric constant would cause power loss if used in MOS devices and thus it is expected that this chapter's discussion of capacitance measurement of oxide thickness will apply to alternate dielectrics. There is little data on the low frequency (<1 GHz) dielectric constant of alternate gate dielectric materials other than book values of the real part of bulk materials. At this time, optical modeling of the interfacial effects is more developed than was that of the interfaceless, slab dielectric model used for calculating thickness from electrical measurements. As discussed above, the optical properties of the interface are

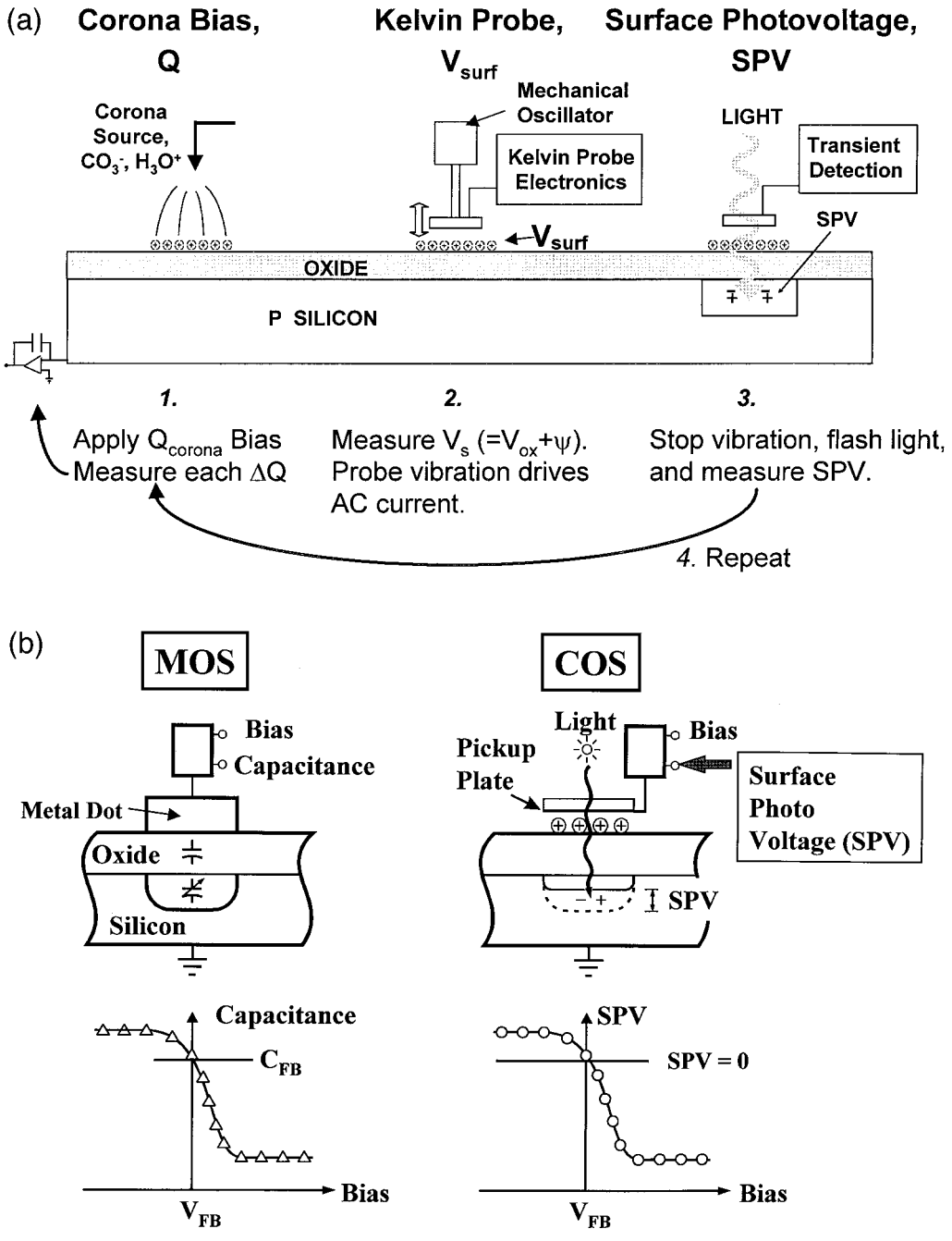

Fig. 35. Comparison of traditional capacitance–voltage with Quantox™ *Q–V*–SPV measurements. (Figure first published in Ref. [71]. Reproduced with permission.) Figure courtesy of Steve Weinzierl, Keithley instruments and verified by Jason Schneir of KLA-Tencor.

different from bulk SiO_2 and thus the dielectric constant of the interface must be different. Both the refractive index and the dielectric constant are frequency dependent quantities. The error in SiO_2 thickness that results from the error associated with the refractive index of bulk silicon at wavelengths used by commercial ellipsometers has been discussed in the literature [14,86]. This leads to the question of how well the static dielectric constant of SiO_2 is known. Direct comparison of both methods requires accurate dielec-

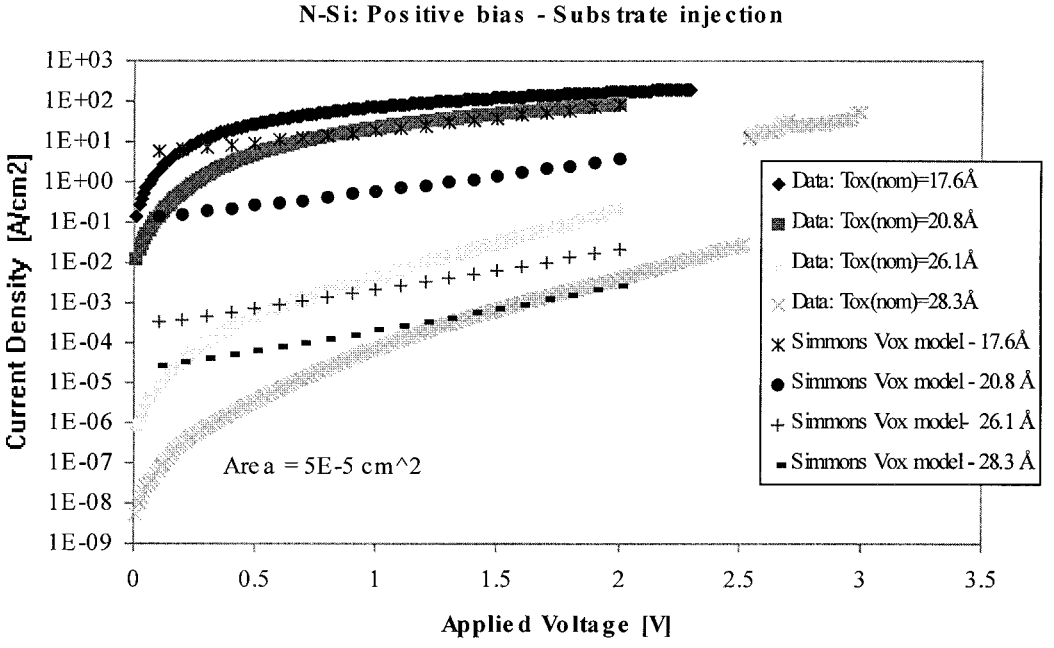

Fig. 36. Current–voltage data applied to oxide thickness measurement. (Figure first published in Ref. [71]. Reproduced with permission.) At 1 V bias, the current varies over seven orders of magnitude as the oxide thickness changes from ~3 to ~1.8 nm. Simulated data is also shown. Figure and data courtesy of George Brown, Texas Instruments.

tric constants at both optical wavelengths and zero frequency. A recent study has investigated the effect of correcting the area used in capacitance-based thickness measurement for the microroughness based increase in area [102]. The proposed correction factor is a function of rms roughness and was calculated to be a small percentage of the total area for rms values below 1 nm [102]. Further work in this is expected to better define the correlation between electrical and physical measurements.

Several workers anticipate a change in the physical structure of the interface after thermal processing done subsequently to gate dielectric oxidation. Some of the predicted structural changes include stress relief, reduction in the amount of substoichiometric oxide states and microscopic smoothening. The change in optical properties associated with these structural changes may result in more uniform dielectric properties thus minimizing the influence of the 'as-grown' interfacial layer. This leads to a complicated set of comparison criteria. For example, ellipsometry and corona discharge based, non-contact C–V method (Quantox™) both measure the gate dielectric after its formation. Transistor based C–V measurements are done after additional thermal processes such as polysilicon gate electrode deposition. Lower temperatures are used for metal electrode (typically aluminum) deposition for C–V test structures. As previously mentioned, the interfacial layer is now a significant part of the total film thickness and differences due to subsequent processing can effect the accuracy of inter-method comparisons and ultimately thickness calibration.

6. Conclusions

The existence of an interfacial layer between silicon

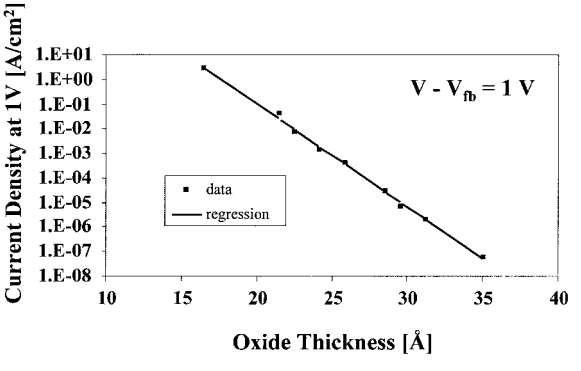

Fig. 37. Current–voltage data with optically measured oxide thickness. (Figure first published in Ref. [71]. Reproduced with permission.) The current values were taken from data at an effective bias (applied voltage–flat band voltage) of 1 V. Figure and data courtesy of George Brown, Texas Instruments.

dioxide and silicon is accepted by a majority of the technical community and this review supports that consensus. There is clearly 1 ML of an interfacial layer in the SiO_2/Si case since it is chemically impossible to go from a Si^{+4} layer to a Si^0 one without having at least one sub-oxide layer. The issue is the extent and nature of the interface beyond this monolayer. There is evidence for up to ~1 ML of additional substoichiometric oxide located within the first 5–10 Å of the interface. Since each characterization method probes slightly different aspects of the interface, we summarize here how they all complement each other to give a more comprehensive picture of the interface stoichiometry, roughness and stress.

X-ray photoelectron spectroscopy shows the presence of at least a monolayer film of incompletely oxidized silicon (known as the sub-oxide layer). The proof of the existence of this layer is based on the assignment of the intermediate region of the Si photoelectron spectrum in terms of incomplete oxidation states, i.e. Si 2p (+3), (+2) and (+1), for data taken on very thin oxide layers of as-deposited films. Electron energy loss studies using scanning transmission electron microscopy show that the shape of both Si–L and O–K edges changes at the interface due to the presence of interface states. Infrared spectroscopy further supports the presence of substoichiometry at the interface.

The issue of atomic level microroughness at the interface over large areas is addressed using ellipsometry and X-ray reflectivity. An area that is microns^2 in size will have many terrace structures and other atomic and larger flatness variations that are called microroughness. Atomic force microscopy typically measures <0.1 nm rms roughness when an area of 1×1 μm is scanned [103]. Larger area scans of 5 μm^2 have observed up to a few tenths of a nm rms [104]. The value of rms depends on tip shape for AFM and comparison with other methods requires knowledge the surface (spatial) wavelength range being sampled. Optical measurements in the visible wavelength range also average this information normal to the surface since the wavelength is large compared to atomic dimensions. Thus ellipsometry observes a slab of mixed dielectric constant. Correspondingly, some scanning transmission electron microscopy and MEIS studies have been interpreted as showing that the silicon below the oxide layer undergoes a lattice expansion of 0.01 and 0.001 nm, respectively.

Stress within the oxide layer itself, i.e. above the interface plane, is also important. Conventional wisdom indicates that the silicon dioxide above the sub-oxide layer is compressively stressed based on the intuitive argument that the SiO_2 lattice has half the Si density as the bulk Si that is being consumed during oxidation. Thus the O_2 induced film growth causes a strain/density change in the overlayer that takes time (and temperature) to relax. X-ray reflectivity and now X-ray photoelectron spectroscopy both support the presence of stress. Earlier IR measurements of the frequency shift of TO and LO upon oxide thinning were also interpreted in terms of oxide stress. The measurements presented in this paper, however, suggest that the TO/LO frequency shifts are in fact dominated by interfacial substoichiometry rather than stress, so that the IR measurements, while consistent with some stress in the oxide, do not bring additional information on the magnitude or nature of the stress. Exciting, X-ray photoelectron spectroscopy data have recently been interpreted in terms of stress in the oxide layer above the sub-oxide region. While acceptance of this new XPS-based observation of stressed oxide awaits critical review by the community, X-ray reflectivity studies are still considered the most accepted evidence for the stressed interfacial oxide layer. One of the models used to describe the X-ray reflectivity data indicates a 1 nm densified (i.e. stressed) oxide layer at the interface. The amount of increase in density over bulk oxide is from 2 to 4%. Another model interprets the X-ray reflectivity data in terms of a much thinner, diffuse interface. This latter model was used in order to facilitate comparison with neutron reflectivity. Despite this ambiguity, the existence of a stressed oxide layer at the interface remains part of the conventional wisdom.

In-line ellipsometry can monitor thickness based on optical models that include an interfacial layer. The question of which model is physically correct remains. The long wavelength of ellipsometry and the need to sample a large area results in an averaged sampling of interfacial optical properties. The next step toward inclusion of a physically correct interfacial layer in the optical model used to interpret in-line ellipsometry is to compare existing interfacial models with one that includes an approximately 1 nm thick interfacial layer with a densified oxide.

Finally, the correlation between electrical measurements such as capacitance–voltage and optical measurements such as ellipsometry requires an improved understanding of the dielectric properties of the oxide film. The dielectric properties of the interface were found to be different from bulk oxide layers and are thought to change after further thermal processing.

Acknowledgements

We gratefully acknowledge Marty Green for his discussion of nitrided oxides and Fig. 14. We also acknowledge Bob Opila, Dick Brundle and Ced Powell for discussion of X-ray photoelectron spectroscopy. ACD would like to acknowledge Dae Won Moon for informing him about the MEIS characterization of thin silicon dioxide and for subsequent discussion

about the interpretation of MEIS. ACD also thanks Jerry Dadap for reviewing the section on optical second harmonic generation and providing figures. We all acknowledge Jim Ehrstein for his contributions concerning optical measurements.

References

[1] Duscher G, Pennycook SJ, Browning ND, Rupangudi R, Takoudis C, Gao H-J, Singh R. Structure, composition and strain profiling of $SiSiO_2$ interfaces. In: Seiler DG, Diebold AC, Bullis WM, Shaffner TJ, McDonald R, Walters EJ, editors. Characterization and metrology for ULSI technology. New York: AIP, 1998. p. 191–6.

[2] Kim YP, Choi SK, Kim HK, Moon DW. Direct observation of Si lattice strain and its distribution in the $Si(001)$–SiO_2 interface transition layer. Appl Phys Lett 1997;71:3504.

[3] Moon DW, Kim HK, Lee HJ, Cho YJ, Cho HM. Thickness of ultrathin gate oxides at the limit. In: Seiler DG, Diebold AC, Bullis WM, Shaffner TJ, McDonald R, Walters EJ, editors. Characterization and metrology for ULSI technology. New York: AIP, 1998. p. 197–200.

[4] Diebold AC, McDonald R. The at-line characterization laboratory of the 90s: characterization laboratories (FAB–LABS) used to ramp-up new FABS and maintain high yield. Future FAB Int 1997;1(3):323–30.

[5] Hattori T. Chemical structure of the SiO_2/Si interface. CRC Crit Rev Solid State Mater Sci 1995;20:339.

[6] Nohira H, Takahashi K, Hattori T. Energy loss of O1s photoelectrons in compositional and structural transition layer at and near the SiO_2/Si interface. In: Heyns M, Meuris M, Mertins P, editors. Proceedings of the Fourth International Symposium on Ultraclean Processing of Silicon Surface (UCPSS98). Scitec, Brandrain, 1998. p. 241–4.

[7] Bjorkman CH, Yamazaki T, Miyazaki S, Hirose M. Characterization of ultrathin SiO_2 films on Si. In: Proc Int Conf Advanced Microelectronic Devices and Processing, 1994. p. 431.

[8] Fitch JT, Lucovsky G, Kobeda E, Irene EA. Effects of thermal history on stress-related properties of very thin films of thermally grown silicon dioxide. J Vac Sci Technol B 1989;7:153.

[9] Yamzaki T, Bjorkman CH, Miyazaki S, Hirose M. Local structure of ultrathin (325 nm) SiO_2 thermally grown on Si(100) and (111) surfaces. In: Proc 22nd Int Conf Phys Semicond, vol. 3, 1994. p. 2653–6.

[10] Hirose M, Mizubayashi W, Fukuda M, Miyazaki S. Characterization of ultrathin gate oxides for advanced MOSFETs. In: Seiler DG, Diebold AC, Bullis WM, Shaffner TJ, McDonald R, Walters EJ, editors. Characterization and metrology for ULSI technology. New York: AIP, 1998. p. 65–72.

[11] Kosowsky SD, Pershan PS, Krisch KS, Bevk J, Green ML, Brasen D, Feldman LC, Roy PK. Evidence of annealing effects on a high-density Si/SiO_2 interfacial layer. Appl Phys Lett 1997;70:3119.

[12] Awaji N, Ohkubo S, Nakanishi T, Sugita Y. High density layer at the Si/SiO_2 interface observed by X-ray reflectivity. Jpn J Appl Phys 1996;35:L67.

[13] Nguyen NV, Chandler-Horowitz D, Amirtharaj PM, Pellegrino JG. Spectroscopic ellipsometry determination of the properties of the thin underlying strained Si layer and the roughness at Si/SiO_2 Interfaces. Appl Phys Lett 1994;64:5599.

[14] Fang SJ, Helms CR. Ellipsometric model studies of the Si surface. Contamination control and defect reduction in semiconductor manufacturing III. Electrochem Soc PV 1994;94(9):267.

[15] Fang SJ, Chen W, Yamanaka T, Helms CR. Influence of interface roughness on silicon oxide thickness measured by ellipsometry. J Electrochem Soc 1997;144:L231.

[16] Fang SJ, Chen W, Yamanaka T, Helms CR. Comparison of Si surface roughness measured by ellipsometry and atomic force microscopy. Appl Phys Lett 1996;68:2837.

[17] Terada N, Haga T, Miyata N, Moriki K, Fujisawa M, Morita M, Ohmi T, Hattori T. Optical absorption in ultrathin silicon oxide films near the SiO_2/Si interface. Phys Rev B 1992;46:2312.

[18] Miyazaki S, Nishimura H, Fukuda M, Ley L, Ristein J. Structure and electronic states of ultrathin SiO_2 thermally grown on Si(100) and Si(111) surfaces. Appl Surf Sci 1997;113–114:585.

[19] Diebold AC. In-line metrology. In: Nishi Y, Doering R, editors. Handbook on semiconductor manufacturing. New York: Dekker, in press.

[20] Batson PE. Nature 1993;366:728.

[21] Timp G, et al. Progress toward 10 mm CMOS devices. In: Proceedings IEDM. 98, 1998. p. 615.

[22] Knapp J, Brice DK, Banks JC. Nucl Instrum Methods B 1996;108:324.

[23] Knapp JA, Banks JC. Proceedings of 12th International Accelerator Conference, Denton, TX, November 25, 1992. Nucl Instrum Methods B, in press.

[24] Arps JH, Weller RA. Nucl Intrum Methods A 1993;B79:539.

[25] Gusev E, Green M, Lu HC, Gustafsson T, Garfunkel E. The chemistry and nano-engineering of silicon oxynitride microelectronic gate dielectrics. J Am Chem Soc, in press.

[26] Gusev E, Lu HC, Gustafsson T, Garfunkel E. Phys Rev B 1995;52:1759.

[27] Lu HC, Gusev E, Gustafsson T, Garfunkel E. Appl Phys 1997;81:6992.

[28] Swanson ML. Surface studies in 'channeling'. In: Tesmer JR, Nastasi M, Barbour JC, Maggiore CJ, Mayer JW, editors. Handbook of modern ion beam materials analysis. Pittsburgh: MRS, 1995. p. 284–95.

[29] Hollinger G, Himpsel FJ. Appl Phys Lett 1984;44:93.

[30] Adachi T, Helms CR. Electron energy loss spectroscopy studies of the $Si–SiO_2$ interface. Appl Phys Lett 1979;35:199.

[31] Nohira H, Hattori T. SiO_2 valence band near the SiO_2/Si(111) interface. Appl Surf Sci 1997;117–118:119.

[32] Nohira H, Omura A, Katayama M, Hattori T. Valence

band edge of ultrathin silicon oxide near interface. Appl Surf Sci 1998;123–124:546.
[33] Ohishi K, Hattori T. Periodic changes in SiO_2/Si(111) interface structures with progress of thermal oxidation. Jpn J Appl Phys 1994;33:L675.
[34] Feldman LC, Gusev EP, Garfunkel E, Ultrathin dielectrics in silicon microelectronics. In: Garfunkel E, Gusev E, Vul A, editors. Fundamental aspects of ultrathin dielectrics on Si-based devices. NATO Science Series 3 High Technology, vol. 47. Netherlands: Kluwer, 1998. p. 1–24.
[35] Opila RL, Chang JP, Du M, Bevk J, Ma Y, Weldon M, Chabal Y, Gurevich A. X-ray photoelectron study of gate oxides and nitrides. In: Heyrts M, Meuris M, Mertins P, editors. Proceedings of Fourth International Symposium on Ultraclean Processing of Silicon Surface (UCPSS98). Scitec, Brandrain, 1998. p. 257–60.
[36] Banaszak Holl MM, McFeely FR. Phys Rev Lett 1993;71:2441.
[37] Banaszak Holl MM, Lee S, McFeely FR. Appl Phys Lett 1994;75:1097.
[38] Pasquerello A, Hybertsen MS, Car R. Phys Rev B 1996;53:10942.
[39] Green ML, Brasen D, Sapjeta BJ, Sorsch TW, Timp G, Lennard WN, Gusev E, Lu HC, Garfunkel E, Gustafsson T, Growth of silicon oxynitride films in NO–O_2 gas mixtures. In: Huff HR, Tsuya H, Gosele U, editors. Proceedings of the Eighth International Symposium on Silicon Materials Science and Technology. Electrochem Soc Proc, vol. 98-1, 1998. p. 745.
[40] Lu ZH, McCaffrey JP, Brar B, Wilk GD, Wallace RM, Feldman LC, Tay SP. SiO_2 film thickness metrology by X-ray photoclectron spectroscopy. Appl Phys Lett 1997;71:2764.
[41] Sipe JE, Moss DJ, van Driel HM. Phenomenological theory of optical second and third harmonic generation from cubic centrosymmetric crystals. Phys Rev B 1987;35:1129.
[42] Dadap JI, Doris B, Deng Q, Downer MC, Lowell JK, Diebold AC. Randomly oriented Angstrom-scale microroughness at the Si(100)/SiO_2 interface probed by optical second harmonic generation. Appl Phys Lett 1994;64:2139.
[43] Dadap JI, Choo HR, Hu XF, Deng Q, Downer MC. Femtosecond ellipsometry and surface second harmonic probes of Ge, Si_{1-x}, Ge_x, Si and diamond. SPIE October 1994.
[44] Cundiff ST, Knox WH, Baumann FH, Evans-Lutterodt KW, Tang MT, Green ML, van Driel HM. Si/SiO_2 interface roughness: comparison between surface second harmonic generation and X-ray scattering. Appl Phys Lett 1997;70:1414.
[45] Bjorkman CH, Shearon CE, Ma Y, Yasuda T, Lucovsky G, Emmerichs U, Meyer C, Leo K, Kurz H. Second-harmonic generation in Si–SiO_2 heterostructures formed by chemical, thermal and plasma-assisted oxidation and deposition processes. J Vac Sci Technol A 1995;13:607.
[46] Lucovsky G, Niimi H, Koh K, Lee DR, Jing Z. In: Massoud HZ, Poindexter EH, Helms CR, editors. Nitrogen at Si–SiO_2 interfaces: chemical bonding and electrical performance, the physics and chemistry of SiO_2 and the Si–SiO_2interface. Pennington, NJ: Electrochemical Soc, 1996. p. 441.
[47] Bjorkman CH, Yasuda T, Shearson CE, Ma Y, Lucovsky G, Emmerichs U, Meyer C, Leo K, Kurz H. The influence of surface roughness on the electrical properties of Si–SiO_2 interfaces and on second harmonic generation at these interfaces. J Vac Sci Technol B 1993;11:1521.
[48] Heinz TF, Loy MMT, Thompson WA. Study of symmetry and disordering of Si(111)-7 × 7 surfaces by optical second harmonic generation. J Vac Sci Technol B 1985;3:1467–70.
[49] Stefanov BB, Gurevich AB, Weldon MK, Raghavachari K, Chabal YJ. Silicon epoxide: unexpected intermediate during silicon oxide formation. Phys Rev Lett 1998;81:3908.
[50] Berreman DW. Phys Rev 1963;130:2193.
[51] Lucovsky G, Galeener FL. In: Kolomicts BT, editor. Structure and properties of non-crystalline semiconductors. Leningrad: Nauka, 1976. p. 207.
[52] de Leeuw SW, Thorpe MF. Coulomb splittings in glasses. Phys Rev Lett 1985;55:2879.
[53] Lehmann A, Schumann L, Hübner K. Optical phonons in amorphous silicon oxides. Phys status solidi (b) 1984;121:505.
[54] Sen, Thorpe. Phonons in AX2 glasses: from molecular to band-like modes. Phys Rev B 1977;15:4030.
[55] Laughlin RB, Joannopoulos JD. Phonons in amorphous silica. Phys Rev B 1977;16:2942.
[56] Thorpe MF. Effect of local order on phonon density of states. Phys Rev B 1973;8:5352.
[57] Kulas R, Thorpe MF. In: Structure and excitations of amorphous solids. New York: American Institute of Physics, 1976. p. 251.
[58] Pasquarello A, Car R. Dynamical charge tensors and infrared spectrum of amorphous SiO_2. Phys Rev Lett 1997;79:1766.
[59] Kirk CT. Quantitative analysis of the effect of disorder-induced mode coupling on infrared absorption in silica. Phys Rev B 1988;38:1255.
[60] Aspnes DE, Theeten JB. Investigation of effective-medium models of microscopic surface roughness by spectroscopic ellipsometry. Phys Rev B 1979;20:3292.
[61] Weldon MK, Chabal YJ, Gurevich AB, Queeney KT, Green ML, Opila RL. Appl Phys Lett, submitted for publication.
[62] Ohwaki T, Takeda M, Takai Y. Characterization of silicon native oxide formed in SC-1, H_2O_2 and wet ozone processes. Jpn J Appl Phys 1997;36:5507.
[63] Devine RAB. Structural nature of the Si–SiO_2 interface through infrared spectroscopy. Appl Phys Lett 1996;68:3108.
[64] Olsen JE, Shimura F. Infrared spectroscopy of thin silicon dioxide on silicon. Appl Phys Lett 1988;53:1934.
[65] Weldon MK, Stefanov BB, Raghavachari K, Chabal YJ. Initial H_2O-induced oxidation of Si(100)-(2 × 1). Phys Rev Lett 1997;79:2851.
[66] Shindler JD, Suter RM. Rev Sci Instrum 1992;63:5343.
[67] Dura JA, Majkrzak CF. In-situ neutron reflectivity of

MBE-grown and chemically processed surfaces and interfaces. In: Bullis WM, Seiler DG, Diebold AC, editors. Semiconductor characterization: present status and future needs. Woodbury: AIP, 1996. p. 549–54.
[68] Richter CA, Nguyen NV, Dura JA, Majkrzak CF. Characterization of thin SiO_2 on Si by spectroscopic ellipsometry, neutron reflectometry and X-ray reflectivity. In: Seiler DG, Diebold AC, Bullis WM, Shaffner TJ, McDonald R, Walters EJ, editors. Characterization and metrology for ULSI technology. New York: AIP, 1998. p. 185–9.
[69] Dura JA, Richter CA, Majkrzak CF, Nguyen NV. Neutron reflectometry, X-ray reflectometry and spectroscopic ellipsometry characterization of thin SiO_2 on Si. Appl Phys Lett, in press.
[70] Berk NF. Outline of neutron scattering formalism. J Res Nat Inst Stand Technol 1993;98:15.
[71] Diebold AC. In-line metrology. In: Nishi Y, Doering R, editors. Handbook of semiconductor manufacturing, 1999, in press.
[72] Tompkins HG. A user's guide to ellipsometry. New York: Academic Press, 1993.
[73] Aspnes DE, Theeten JB, Hottier F. Investigation of effective-media models of microscopic surface roughness by spectroscopic ellipsometry. Phys Rev B 1977;20:3513.
[74] Aspnes DE, Theeten JB. Spectroscopic analysis of the interface between Si and its thermally grown oxide. J Electrochem Soc 1980;127:1359.
[75] Opsal J, Fanton J, Chen J, Leng J, Wei L, Uhrich C, Senko M, Zaiser C, Aspnes DE. Broadband spectral operation of a rotating-compensator ellipsometer. Thin Solid Films 1998;313/314:58.
[76] Corle TR et al. A broadband UV small spot spectroscopic ellipsometer. Paper presented at SPIE Microlithography, Integrated Circuit Metrology Inspection and Process Control IX. SPIE, 1995. p. 2439.
[77] A description of the Rudolph simultaneous multi-angle, multiple wavelength system technology can be found in US Patent No. 5166752.
[78] Diebold AC, Doris B. Survey of non-destructive surface characterization methods used to insure reliable gate oxide fabrication for silicon IC devices. Surf Interface Anal 1993;20:127.
[79] Malitson IH. Opt Soc Am 1965;55:1205.
[80] Aspnes DE, Studna AA. Dielectric functions and optical parameters of Si, Ge, GaP, GaAs, GaSb, InP, InAs and InSb from 1.5 to 6.0 eV . Phys Rev B 1983;27:985.
[81] Jellison Jr GE. Optical functions of silicon determined by two-channel polarization modulation ellipsometry. Opt Mater 1992;1:41.
[82] Aspnes DE, Theeten JB. Optical properties of the interface between Si and its thermally grown oxide. Phys Rev Lett 1979;43:1046.
[83] Herzinger CM, Johs B, McGahan WA, Woollam JA, Paulson W. Ellipsometric determination of optical constants for silicon and thermally grown silicon dioxide via a multi-sample, multiwavelength, multiangle investigation. J Appl Phys 1998;83:3323.
[84] Hu YZ, Tay SP, Wasserman Y, Zhao CY, Hevert KJ, Irene EA. Optical properties of the interface between Si and its thermally grown oxide. J Vac Sci Technol A 1997;15:1394.
[85] Nayar V, Pickering C, Hodge AM. Determination of properties of thin thermal SiO_2 on silicon by spectroscopic ellipsometry. Thin Solid Films 1991;195:185.
[86] Taft E, Cordes L. Optical evidence for a silicon–silicon oxide interlayer. J Electrochem 1979;126:131.
[87] Chandler-Horowitz D, Candela GA. On the accuracy of ellipsometric thickness determination for very thin films. J Phys C 1983;10:23.
[88] Aspnes DE, Theeten JB. Dielectric function of Si–SiO_2 and Si–Si_3N_4 mixtures. J Appl Phys 1979;50:4928.
[89] Nicollian EH, Brews JR. Metal oxide silicon capacitor at low frequencies. In: MOS (metal oxide semiconductor) physics and technology. New York: Wiley, 1982. p. 71.
[90] Nicollian EH, Brews JR. Metal oxide silicon capacitor at intermediate and high frequencies. In: MOS (metal oxide semiconductor) physics and technology. New York: Wiley, 1982. p. 99.
[91] Blood P, Orton JW. Capacitance–voltage profiling. In: The electrical characterization of semiconductors: majority carriers and electron states. New York: Academic Press, 1992. p. 220.
[92] Emerson NG, Sealy BJ. Capacitance–voltage and hall effect measurements. In: Grasserbauer M, Werner HW, editors. Analysis of microelectronic materials and devices. New York: Wiley, 1991. p. 865.
[93] Schroder DK. Oxide and interface trapped charge. In: Semiconductor material and device characterization. New York: Wiley, 1990. p. 244.
[94] Lee K, Shur M, Fjeldly TA, Ytterdal T. Surface charge and the metal insulator semiconductor capacitor. In: Semiconductor device modeling for VLSI. Englewood Cliffs: Prentice-Hall, 1993. p. 196.
[95] Hauser JR, Ahmed K. Characterization of ultrathin oxides using electrical C–V and I–V measurements. In: Seiler DG, Diebold AC, Bullis WM, Shaffner TJ, McDonald R, Walters EJ, editors. Characterization and metrology for ULSI technology. New York: AIP, 1998. p. 235–9.
[96] Reisinger H, Oppolzer H, Honlein W. Thickness determination of thin SiO_2 on silicon. Sollid-State Electron 1992;35:797.
[97] Schenk A, Heiser G. Modeling and simulation of tunneling through ultrathin gate dielctrics. J Appl Phys 1997;81:7900.
[98] Song H, Dons E, Sun XQ, Farmer KR. Leakage compensated charge method for determining static C–V characteristics of ultrathin MOS capacitors. In: Seiler DG, Diebold AC, Bullis WM, Shaffner TJ, McDonald R, Walters EJ, editors. Characterization and metrology for ULSI technology. New York: AIP, 1998. p. 231–4.
[99] Brown G. Private communication.
[100] Weinzeirl S, Schneir J. Private communication.
[101] Ibach H, Luth H. Dielectric properties of materials. In: Solid-state physics. Berlin: Springer-Verlag, 1991. p. 239.
[102] Lin HC, Ying JF, Yamanaka T, Fang SJ, Helms CR. Analysis of interface roughness's effect on metal-oxide-

semiconductor Fowler–Nordheim tunneling behavior using atomic force microscopy images. J Vac Sci Technol A 1997;15:790.
[103] Strausser YE, Doris B, Diebold AC, Huff HR. ECS extended abstracts 94-1. In: Measurement of silicon surface microroughness by AFM, 1994. p. 239.
[104] Huff HR. Private communication.
[105] Aiba T, Yamauchi K, Shimizu Y, Tate N, Katayama M, Hattori T. Initial stages of oxidation of hydrogen terminated Si(100) 2×1 surface. Jpn J Appl Phys 1995;34:707.
[106] Cundiff ST, Knox WH, Baumann FH, Evans-Lutterodt KW, Green ML. Second-harmonic generation at the interface between Si(100) and thin SiO_2 layers. J Vac Sci Technol A 1998;16:1730.
[107] Heinz TF, Loy MMT, Thompson WA. Study of Si(111) surfaces by optical second harmonic generation: reconstruction and surface phase transformation. Phys Rev Lett 1985;54:63.
[108] Galeener FL, Lucovsky G. Phys Rev Lett 1976;37:1474.
[109] Phillip HR. J Phys Chem Solids 1971;32:1935.
[110] Sarnthein J, Pasquarello A, Car R. Origin of high-frequency doublet in the vibrational spectrum of vitreous SiO_2. Science 1997;275:1925.
[111] Aspnes DE. Local field effects and effective medium theory: a microscopic perspective. Am J Phys 1982;50:704.
[112] Knapp JA, Barbour JC, Doyle BL. J Vac Sci Technol A 1992;10:2685.